NATIONAL DEFENSE INDUSTRIAL ASSOCIATION

STRENGTH THROUGH INDUSTRY & TECHNOLOGY

US Army Ground Vehicle Survivability Symposium

29 Mar-1 Apr 1999

Approved for public release.
Distribution is unlimited

19991028 024

US Army Ground Vehicle Survivability Symposium

29 Mar-1 Apr 1999

Table of Contents

ESTIMATION OF VEHICLE FLOOR PLATE LOADING AND RESPONSE DUE TO DETONATION OF A MINE SHALLOW-BURIED IN DRY SAND AND WET TUFF (U)

Aaron D. Gupta
U.S. Army Research Laboratory
Aberdeen Proving Ground, Maryland

ABSTRACT

(U) A mine-soil-structure interaction problem with a landmine buried in two different soil types was modeled using a hydrodynamic code. Because the actual soil types can vary widely between experiments, the problem was bracketed between two widely differing soil types— dry sand and fully saturated tuff. The ballistic pendulum anvil plate acts as a momentum trap for a vertical impulse measurement facility (VIMF) under development at Aberdeen Proving Ground, MD. The model allows simulation of complex asymmetric explosive-soil-structure interaction effects. It also generates loading and response of the plate due to varying offset, standoff, depth of soil overburden, and explosive contents.

(U)   Introduction

(U)   Both armored personnel carriers and light combat vehicles are increasingly being used in a support role for other, more heavily armored combat vehicles, all of which are being subjected to much greater risk from a variety of highly lethal antitank land mines. As a result, there is a need for modeling and understanding the interaction of mine blast products with structures and the resulting loading and damage mechanisms inflicted by explosive blast and impact. This understanding is required both for damage assessment and protective hardening of both wheeled and tracked vehicles. This has been a topic of considerable interest to the U.S. Army Research Laboratory (ARL) at Aberdeen Proving Ground, MD.

(U)   An interesting study [1] involved collation of data from previous scaled experiments related to the encounter of buried land mines with various targets including flat plates. A correlation function, based on dimensional analysis, for the total impulse delivered by the land mine and overburden on a target was presented. Vulnerability of tank bottom hull floor plates subjected to shallow-buried mine blast was studied by Norman [2] and Hoskins et al. [3], who employed an approximate energy method approach and equated the strain energy absorbed by the plate to the energy delivered by the blast to the armor plate based on the law of conservation of energy. Various simple models of explosively driven metal were developed by Dehn [4] and compared with experiments.

(U)   In another investigation [5], the DORF hydrocode was used to generate the loading history on a target plate subjected to a blast load from a land mine. The forcing function was used to compute the response of a clamped-edge square rolled homogeneous armor (RHA) plate using a structural response code. The predicted deflection and total impulse were in satisfactory agreement with values computed using an empirical correlation function derived from field experimental data.

(U)   Dynamic response analysis of a rectangular simply supported plate subjected to an explosive blast was analyzed by Gupta [6] for the linear elastic case and compared to a closed-form solution. The analysis was extended to the elastic-plastic domain by Gupta et al. [7], who employed the isotropic bilinear hardening material model available in the ADINA nonlinear finite element analysis code. This study was further extended by Gupta et al. [8] to the response of a generic vehicle floor model subjected to empirically obtained triangular overpressure loads from the detonation of a shallow-buried mine. Although qualitative agreement with experiment for peak deflection could be obtained, the residual plastic deformation could not be compared effectively due to lack of soil loading arising from blast-soil-structure interaction, which substantially affected the estimated blast loads and the resultant structural response. Another recent study of dynamic elastic-plastic stress and deformation response of a generic vehicle floor model to coupled blast and impact loads from a plate mine was reported by Gupta [9], who provided an inexpensive method of evaluation of the structural integrity of modern vehicles subjected to severe spatially varying transient loads in extreme environments.

(U)   A number of studies have been performed in the general area of blast response to structures over the years. However, the loading mechanisms from explosive blast-soil-structure interaction such as those occurring from detonation of a buried mine below a vehicle are poorly understood at present. The current investigation is an attempt to fill this void and to simulate loading of the anvil plate, which acts as a momentum trap due to an off-centered mine explosion and subsequent blast-soil-structure interaction resulting in target rotation and vertical displacements needed for the design of the guide shaft for the Vertical Impulse Measurement Facility (VIMF).

(U)   Objective

(U)   The primary objective of this investigation is to simulate detonation of a mine buried

in two different soil types—saturated tuff and dry sand. The shallow-buried mine detonation causes motion of the soil media and propagation of the blast-soil wave upward, resulting in blast-soil-structure interaction and consequent loading of the anvil plate, which is employed as a momentum trap. The study is necessitated by the need to obtain improved loading functions for combined blast and soil loading under extreme loading conditions and bracket the influence of soil properties upon the loading and response of the ballistic pendulum anvil plate between two differing soil types and moisture contents. These loading data can then be transferred to a nonlinear finite element analysis code to yield transient structural response including deformation, displacement, and rotation of a representative structural element. The predicted results could then be compared to data from experiments designed to capture and measure the loads produced in these events in a severe environment. Such capability will, in turn, enable the development of models of expansion of blast/soil events in which soil properties play a significant role.

(U)   Accuracy of predictive models is essential to the development of innovative vehicle designs that have improved survivability characteristics and are, at the same time, light enough to ensure rapid deployment and desired load-carrying capacity. The ultimate objective is to improve survivability of crew in vehicles subject to land mine attack.

(U)   Problem Configuration

(U)   The problem involves the worst-case scenario of a shallow-buried cylindrical mine embedded all around in two different soil types: dry sand and wet soil with a 15-cm soil overburden. The mine contains explosive with an equivalent charge weight of 10 kg TNT and is asymmetrically located with a horizontal centerline offset distance of 61 cm relative to a square plate 244 cm H 244 cm. Plate thicknesses of 15 cm and 20 cm were modeled. The vertical standoff between the bottom plate surface and the top of the soil overburden was 41 cm as shown in Figure 1. The cylindrical configuration of the mine has a diameter of 32 cm and a height of 9 cm. The mine is located inside a block of soil 366 cm in diameter with a total height of 124 cm.

(U)   Basic Assumptions

(U)   The asymmetric configuration of the mine as defined in the previous section is a three-dimensional (3-D) problem requiring the generation of a 3-D model that is expensive to run using a hydrodynamic code. The model was simplified using two-dimensional (2-D) plane strain assumptions. In this model, lateral dimensions of the plate, the mine, and the soil enclosure perpendicular to the X-Y plane were assumed to extend to infinity.

(U)   The mine is assumed to consist of a bare charge without the presence of a metallic casing. The relatively small mass of the casing would not significantly contribute to the resultant impulse or momentum absorbed by the momentum trap. The plate is expected to undergo minimal deformation in order that displacements and rotations can be easily tracked and compared with experiments.
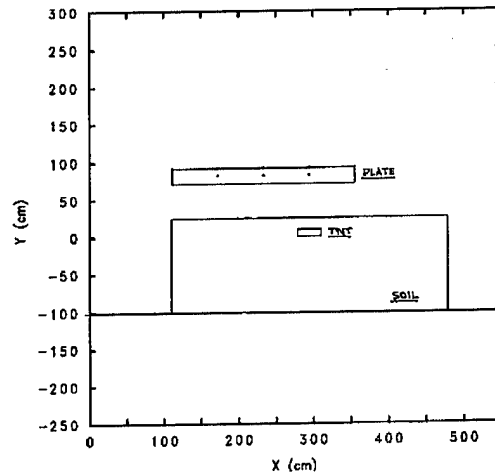
Figure 1. (U) Initial Configuration of the Mine-Soil-Structure Interaction Problem

UNCLASSIFIED

(U)   All empty spaces between the plate and the soil block and all around these configurations were filled with dry air in the hydrocode model. The fully saturated tuff is assumed to be strongly clumped together due to high moisture content completely filling the void volume, which is approximately 30% of the entire soil volume. This ensures a worst-case scenario with significant contribution to the resultant momentum produced in the momentum trap. In the second case, dry sand with no moisture content is considered as the burial medium. This allows bracketing of the influence of large variation of soil properties and moisture contents upon structural loading and response between two widely varying soil types.

(U)   Model Description

(U)   A 2-D asymmetric model with a 61-cm centerline offset of the anvil plate, as shown in Figure 1, was generated for the CTH code. A 2-D Eulerian mesh was overlaid using uniform grid spacing in both horizontal and vertical directions throughout the computational space. Each cell size was a square mesh 1 cm × 1 cm, and the total number of cells was 165,000. An aspect ratio of 1.0 was maintained in computational space to ensure numerical accuracy. The problem region was extended approximately 110 cm vertically above the top plate surface and horizontally beyond the left and right geometric edges to minimize reflection from the computational boundaries. This large

volume of space filled with dry air accommodated large displacements and tilt angles of the anvil plate expected to occur due to asymmetric loading from mine detonation. Computed prediction of peak vertical displacements and rotation will be useful in designing vertical guides, guide bars, and springs for the experimental test fixture.

(U)   Boundary Conditions

(U)   The steel plate is assumed to be freely suspended 46 cm above the top surface of the soil block in which the mine is embedded and is initially at rest. The bottom horizontal soil boundary 100 cm below the mine is assigned a transmitting boundary condition where mass may flow in and out of mesh but no reflection is allowed from the boundary.

(U)   Both left and right vertical as well as the top horizontal boundaries of the computational mesh are assigned extrapolated pressure boundary conditions where mass is not allowed to flow into the mesh but the pressures in cells at the boundary are computed using extrapolated values from two adjacent cells. This boundary condition is mostly transmissive with some reflection permitted.

(U)   Material Models

(U)   The model involves four different material types. The first package in the problem setup represents the TNT explosive for the land mine. The next package represents the rolled homogeneous armor (RHA) steel plate. This is followed by the soil package surrounding the explosive. The final package refers to dry air, which is used to fill all remaining empty space between and around the previous three packages and extends up to the edges of the computational mesh.

(U)   The Mie-Grüneisen equation of state for steel available from the CTH code [10] material library was used to model the anvil plate. The corresponding response of the plate appeared to be highly dependent on material density rather than the assigned Grüneisen coefficients, and no attempt was made to improve upon these coefficients to better represent the RHA steel.

(U)   Initially, the Johnson-Cook [11] constitutive model for the deviatoric response behavior of steel was used, which resulted in appreciable transverse bending deformation of the steel plate. To simulate nearly rigid deformation response of the steel plate, an elastic-perfectly plastic constitutive relationship with a high yield point and a high initial elastic modulus was used. This model appeared to work reasonably well since rigid-body translation and rotation of the steel plate were of primary interest.

(U)   The material model employed for the TNT explosive was the JWL (Jones-Wilkins-Lee) equation of state available in the material library. For the detonation of the explosive, an explosive burn routine designated as HEBURN in the hydrocode was employed. The initiation was chosen to start at the bottom central location on the vertical symmetry axis of the mine, and pressure contour plots were generated at a regular interval of 10-cm radius.

(U)   The soil material models were rather difficult to select because of limited information available on dynamic soil properties of widely differing soil types at high strain rates. Soil properties appear to vary considerably depending upon the location, type, moisture content, porosity, aggregate size, ambient temperature, and humidity conditions, etc. These property variations can significantly affect the interacting loading mechanisms and generated load functions as well as the resultant structural response. Most dynamic soil equations of state are devoted to high compression regimes appropriate in underground tests, and very little information is available for soil models in tension or dilatation as occurs in shallow-buried mine explosions.

(U)   After consideration of various soil types, two different soil types were selected to bracket the problem between two limiting soil conditions. The soil types selected were fully saturated tuff designated as WTUFF and dry sand whose material models are available in the CTH Seslan material library. The equation of state for wet tuff has all voids filled with water. The void volume is approximately 30% of the total volume. The soil is assumed to remain clumped together during blast propagation and interaction with the target for a considerable period of time until the combined soil and blast products flow past the target corners and envelop the front and side surfaces of the anvil plate. Reasonably high fracture strength was specified for WTUFF to minimize severe fragmentation of the soil and allow maximum vertical momentum to be imparted to the anvil plate. The yield strength for wet soil was set at a realistic value, which was an order in magnitude lower than the fracture strength.

(U)   The equation of state for dry sand available in the material library was similar to quartz crystal with an initial density of 2.6 cm^3, which was deemed to be too high. The dry sand appeared to behave like a rock with high density and stiffness properties. The high density and low porosity contributed to unrealistic mass and momentum to be imparted to the anvil plate acting as a momentum trap. The porosity ratio was reset at 1.45 in the model, and the CTHGEN preprocessor was rerun to produce the correct density and mass, plus a pressure that was essentially ambient. After model verification, CTH was rerun with the improved dry sand model. Since the dry sand was initially in contact with the mine at rest, it evolved along with the blast wave from mine detonation. The resultant blast-soil wave propagated together toward the anvil plate, and numerical instability was not a problem.

(U)   Response Computation

(U)   The simulation of the propagation of the explosive blast and soil products through the air and of the subsequent interaction with the steel plate was performed using the CTH hydrodynamic code. An initial time step of 1.0 μs was selected at the start of computation, and the response was tracked up to 2 ms, corresponding to approximately 2,000 computational cycles. A minimum time step of 0.01 μs was specified to avoid numerical instability.

(U)   Gravity effects were included in the simulation to duplicate actual experimental conditions. Active Lagrangian tracer particles were selected along the back surface and the

horizontal midplane as well as the vertical axis of symmetry of the plate. The selection of tracer particles where history plots of position, velocity, pressure, and maximum principal stress as a function of time would be generated was guided by experimental considerations. The locations selected generally corresponded with locations where gauges were to be mounted.

(U)   History plots of vertical linear momentum trapped in the RHA steel plate were generated for later comparison with momentum measurements. Cross-sectional plots of blast-soil-structure interaction and target response were plotted at frequent time intervals. These graphical representations led to a better understanding of the loading mechanisms.

(U)   Results and Discussions

(U)   Cross-sectional plots of blast-soil-plate interaction revealed elongation of steel plate at bottom corners in spite of high elastic modulus and stiffness properties of the RHA steel. Corner deformation was found to be an artifact of the numerical code computation, occurring at or near the interface where a mesh containing a relatively stiff material is located next to a soft material. This condition caused uncontrolled material flow and leakage through corners along the interface. It was decided to use the boundary layer interface (BLINT) capability in the code along the interface between the hard RHA steel target and the relatively soft air medium to mitigate this problem. However, no significant change was observed in the resultant time history or cross-sectional plots due to use of the BLINT capability available in the hydrocode.

(U)   Two alternative plate thicknesses—15 cm and 20 cm—were considered. The objective was to find an optimum thickness for the anvil plate capable of trapping the momentum without significant bending deformation but yet yielding measurable rise in height. Computation using the 15-cm-thick anvil plate exhibited significant bending deformation, a typical cross-sectional view of which is shown in Figure 2. The amount of deformation observed was deemed unacceptable.

(U)   Computations using the 20-cm-thick plate exhibit only minimal bending deformation, a typical cross-sectional plot of which is shown in Figure 3. This figure also depicts visible tilting of the plate. Both vertical and horizontal displacements of tracers on the rear surface, midplane, and the vertical plate symmetry axis were generated to facilitate calculation of peak displacements and tilt angles of the plate at specific response times.

(U)   A typical history plot of integrated linear momenta in the vertical Y direction for the steel plate is shown in Figure 4. The momentum is initially 0 for the first 0.5 ms until the arrival of the blast wave at the bottom interface of the plate. The momentum absorbed by the plate increases rapidly for the next 0.1 ms and then gradually for an additional 1.4 ms. Thereafter, it reaches a plateau before eventually decaying due to air drag and gravitational effects. Comparison of the anvil plate vertical momenta from detonation of a mine buried in saturated tuff (shown as a curve joining filled diamonds) vs. dry sand (described by a curve joining square boxes) indicates consistently higher momenta for wet tuff relative to dry sand attaining a peak differential of between approximately 25% and 30% as shown in Figure 4. This is not unexpected since dry sand has a significantly lower density

than wet tuff, which remains cohesive for a considerable period of time before fragmentation while
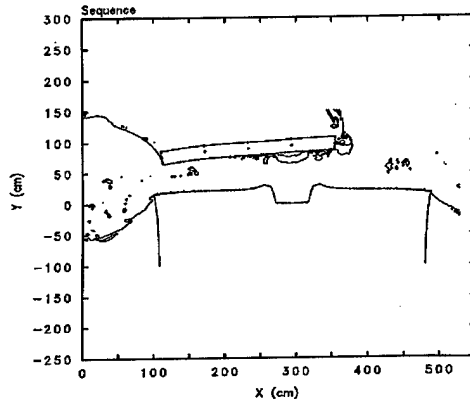UNCLASSIFIED

Figure 2. (U) A Sectional View of the Mine-Soil-Plate Interaction at 2 ms for the 15-cm-Thick Plate
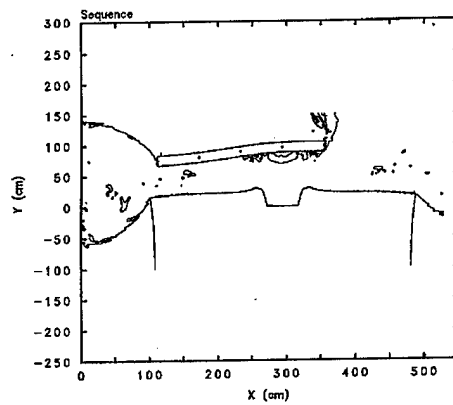
UNCLASSIFIED

UNCLASSIFIED

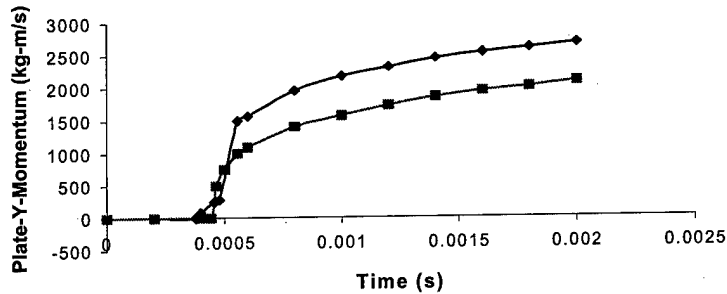Figure 3. (U) A Sectional View of the Mine-Soil-Plate Interaction at 2 ms for the 20-cm-Thick Plate

UNCLASSIFIED

Figure 4. (U) Comparison of Plate Vertical Momentum From Detonation of Mine Buried in Wet Tuff vs. Dry Sand

lighter sand particles have low mass and momentum and tend to separate earlier before reaching the plate surface.

(U)   Section plots of explosive detonation and progression of blast waves leading to interaction with soil ejecta and the anvil plate as well as history plots of pressure, velocity, stress, and impulse are available but are not presented here due to space limitation. However, these plots indicate a thin layer of soil located near the leading edge of the blast wave, which is eventually compressed and flattened out against the anvil plate. Subsequently, the blast wave front branches out laterally along the plate interface until it reaches the bottom plate corners on either side. The wave then flows around these corners and envelops the plate. The bottom right corner is engulfed first because of its proximity to the wave front due to asymmetric location of the plate relative to the buried explosive. The asymmetric nature of blast wave interaction with the plate results in nonuniform loading of the plate. This leads to angular tilting, which is clearly visible in Figure 5.

(U)   The vertical rise of the anvil plate due to entrapment of the linear vertical momentum shown in Figure 4 is accompanied by simultaneous rotation of the plate due to asymmetric loading of the plate from the blast-soil-structure interaction. The amount of rotation of the plate could not be predicted explicitly by the CTH code. However, data output tables of both vertical and horizontal locations of the tracer particles numbered 1–5 on the central horizontal plate axis, with respect to time, could be generated easily in a two-column ASCII format in CTH and readily transferred to Excel 97. A straight line equation of the form y = mx + c (where m is the gradient and c is the intercept) was fitted at each selected response time. Angular rotation of the fitted line was calculated in radians and converted to degrees from the relationship of the form m = tan[(180/pi) H theta],
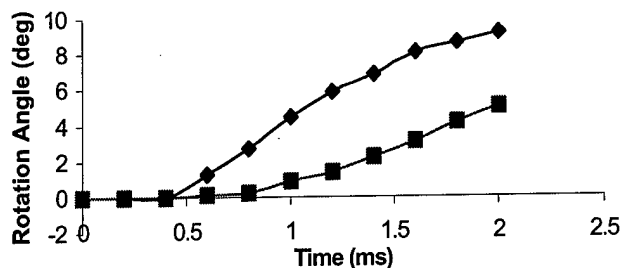
Figure 5. (U) Comparison of Rotation Angles Between 15-cm and 20-cm-Thick RHA Plates vs. Time Due to Detonation of a Mine Buried in Saturated Tuff

where theta is the angle of rotation. Plots of rotational angles of the plate median axis with time for the 20-cm-thick plate vs. the 15-cm-thick plate due to detonation of the mine buried in wet tuff were generated in Excel and superimposed as shown in Figure 5. The curve connecting rectangular-filled boxes refer to the 20-cm-thick plate while the other curve represents the 15-cm-thick plate. Peak tilt angle for the 15-cm-thick plate was nearly twice the peak angle for the 20-cm-thick plate. Comparison of angular tilt for the 20-cm-thick plate due to the mine embedded in dry sand vs. wet tuff is shown in Figure 6. Although the plate shows higher tilting initially due to mine detonation in sand due to early arrival of lighter sand particles, at later times plate rotation due to mine detonation in wet tuff is clearly higher when compared to the response due to sand due to increased mass and momentum of saturated tuff both along vertical and horizontal directions.

(U)   The peak vertical rise of the momentum trap at the midpoint on the axis of symmetry of the plate was obtained from the CTH data output table at the Lagrangian tracer particles by subtracting the initial y-position data from the final vertical location of the tracer particle 3 at 2 ms for both 20-cm-thick and 15-cm-thick plates. The results were tabulated and plotted in Excel 4, and the resultant plot is shown in Figure 6. A linear interpolation has been assumed between these data points, but this may change as more data become available. The vertical momentum plot in Figure 4 reaches a plateau at 2 ms, at which point acceleration is vanishingly small but the residual velocity due to inertia of the plate will continue to allow the plate to rise further until gravity brings the plate to a halt and reverses direction of motion as the plate starts to fall until it returns to the initial position. The 244-cm H 244-cm H 15-cm plate has a total mass of 6,770 kg and a vertical rise of 10.78 cm while the 244-cm H 244-cm H 20-cm plate has a total mass of 9,030 kg and a vertical rise of 7.66 cm at 2 ms. As expected, the thicker plate with an increased mass and moment of inertia

attains a smaller vertical rise at 2 ms as shown in Figure 7.
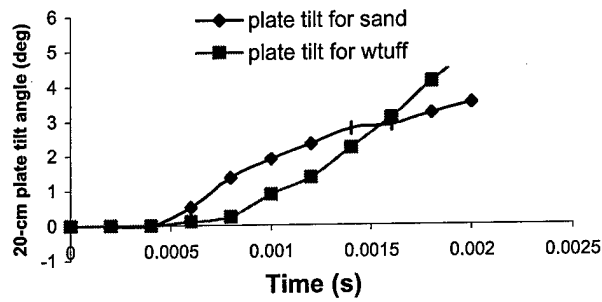
Figure 6. (U) Comparison of 20-cm Plate Rotation Due to Mine Detonation in Dry Sand vs.
Wet Tuff

UNCLASSIFIED

UNCLASSIFIED
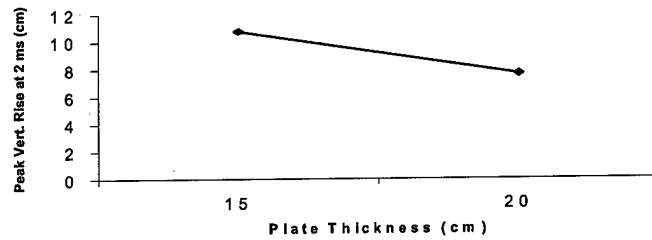
Figure 7. (U) Peak Vertical Rise of the Momentum Trap vs. Plate Thickness at 2 ms

UNCLASSIFIED

(U)   Conclusions and Recommendation

        (U)   The 20-cm-thick RHA plate experienced minimal transient deformation but incurred
a severe weight penalty. To minimize weight, two plates with a total thickness of 10 cm were used.
The loss of stiffness was compensated using two 5-cm-thick plates connected to I-beams in between
with approximately equivalent stiffness of a 20-cm-monolithic plate. This design has the benefit of

easy replacement of the bottom parasitic plate, which is subjected to permanent damage from repeated tests without having to replace the entire momentum trap.

(U)   The selection of soil properties in this study was limited to only two types of soil—dry sand and wet tuff—which were representative of two widely differing soil types and moisture conditions and limited the problem between fully dry and fully saturated soil media. The selection of soil properties must be broadened to include other types of soil with differing moisture contents and porosity. The soil fracture properties need to be improved particularly to include granularity and realistic soil fragmentation as well as ejecta formation. Further parametric studies should be conducted to include different types of landmines with varying types and contents of explosive. Additionally, the effect of varying standoff and offset distances on plate response behavior should be studied and compared with experiments for purposes of model validation. Once these effects are well understood and confidence is gained in modeling and simulation of mine-soil-structure interaction problems, improved design for blast mitigation and crew protection from land mines is feasible.

(U)   Acknowledgements

(U)   This project was undertaken as a part of a program involving land mine effects on structures. The valuable assistance of N. Gniazdowski, P. Kingman, and F. Gregory, of Weapons and Materials Research Directorate, and S. Betten, a George Washington University Science and Engineering Apprentice at ARL, during the course of this investigation is gratefully acknowledged.

(U)   References

1.   (U)   Hanna, J. W. "An Effectiveness Evaluation of Several Types of Antitank Mines." BRL-MR-616, U.S. Army Research Laboratory, Aberdeen Proving Ground, MD, 1952 (UNCLASSIFIED).

2.   (U)   Norman, R. M. "Deformation in Flat Plates Exposed to HE Mine Blast." AMSAA-TM-74, U.S. Army Materiel Systems Analysis Agency, Aberdeen Proving Ground, MD, 1970 (UNCLASSIFIED).

3.   (U)   Hoskin, N. E., J. W. Allan, W. A. Bailey, J. W. Lethaby, and I. Skidmore. "The Motion of Plates and Cylinders Driven at Tangential Incidence." *Fourth International Symposium on Detonation,* ACR-126, Office of Naval Research, Pasadena, CA, 1965 (UNCLASSIFIED).

4.   (U)   Dehn, J. T. "Models of Explosively Driven Metal." BRL-TR-2626, U.S. Army Research Laboratory, Aberdeen Proving Ground, MD, 1984 (UNCLASSIFIED).

5.   (U)   Lottero, R. E., and K. D. Kimsey. "A Comparison of Computed Versus Experimental; Loading and Response of a Flat Plate Subjected to a Mine Blast." BRL-MR-02807, U.S. Army Research Laboratory, Aberdeen Proving Ground, MD, 1984 (UNCLASSIFIED).

6.   (U)   Gupta, A. D. "Dynamic Analysis of a Plate Subjected to an Explosive Blast." *Proceedings of the ASME International Computers in Engineering Conference and Exhibition,* vol. 1, Boston, MA, 1985 (UNCLASSIFIED).

7.   (U)   Gupta, A. D., F. H. Gregory, R. L. Bitting, and S. Bhattacharya. "Dynamic Analysis of an Explosively Loaded Hinged Rectangular Plate." *Computers and Structures,* vol. 26, pp. 339–344, United Kingdom: Pergamon Press Ltd., 1987 (UNCLASSIFIED).

8.   (U)   Gupta, A. D., H. L. Wisniewski, and R. L. Bitting. "Response of a Generic Vehicle Floor Model to Triangular Overpressure Loads." *Computers and Structures,* vol. 32, no. 3/4, pp. 527–536, United Kingdom: Pergamon Press Ltd., 1989 (UNCLASSIFIED).

9.   (U)   Gupta, A. D. "Dynamic Elasto-plastic Response of a Generic Vehicle Floor Model to Coupled Transient Loads." PVP-Vol. 351. *Structures Under Extreme Loading Conditions,* pp. 81-86, ASME, 1997 (UNCLASSIFIED).

10.   (U)   McGlaun, J. M., S. L. Thompson, and M. G. Elrick. "CTH: A Three-Dimensional Shock Wave Physics Code." *International Journal of Impact Engineering,* vol. 10, nos. 1–4, pp. 251–360, 1990 (UNCLASSIFIED).

11.   (U)   Johnson, G. R., and W. H. Cook. "A Constitutive Model and Data Subjected to Large Strains, High Strain Rates and High Temperatures." *Proceedings of the Seventh International Symposium on Ballistics,* pp. 541–547, The Hague, Netherlands, 1983 (UNCLASSIFIED).

ADVANCED TRANSPARENT POLYMER DEVELOPMENT FOR LIGHTWEIGHT TRANSPARENT ARMOR (U)

Richard A. Huyett
Armor Technology Specialist
Simula Technologies, Inc.
Phoenix, Arizona 85044

ABSTRACT (U)

(U)   This paper describes a family of new transparent polyurethane polymers developed by Simula Technologies, Inc.. The new polymers possess improved properties which can significantly reduce the weight of transparent armor used for protection against small-arms projectile, ballistic fragmentation, and laser threats, either singly or in combination. The key properties of the new polymers are presented and compared to currently used materials, such as as-cast acrylic and polycarbonate. The polymer's unique processing characteristics, which facilitate the manufacture of configured eye protection devices and transparent armor for ground vehicles and aircraft, are also discussed.

(U)   The contributions which the new polymers have made to date to several key U.S. Army advanced transparent armor development programs are described. The polymer's planned use within the Army's newly-awarded Advanced Lightweight Transparent Armor program are also presented. A number of design architectures are shown which illustrate the breadth of the polymer's potential usage, both as individual components and as complete transparent armor systems. In addition to weight savings, the polymer's processing characteristics and properties offer the promise of reduced manufacturing costs and improved durability in service.

(U)   Introduction

(U)   Several of the U.S. Army's major thrust programs seek to reduce the weight of transparent armor. The scope of the Army's search for reduced weight solutions for transparent armor runs from individually worn eye protection devices, such as spectacle lenses and visors, to glass/plastic laminates for aircraft and ground vehicles transparencies which are capable of defeating high-velocity small-arms projectiles and ballistic fragments.

(U)   The performance of transparent armor has historically lagged behind that of opaque armor, when judged by the armor's mass-efficiency parameter. The mass-efficiency parameter is the comparative ratio of the transparent armor's areal density to the areal density of a standard armor material, usually steel or

aluminum plate, that is required to defeat the same threat under nominally identical test conditions. The highest-performing transparent armor designed to defeat small-arms projectiles typically consists of a laminated glass / plastic composite. The hard glass striking ply is required to blunt and/or break up the pointed projectile and dissipate a substantial portion of its kinetic energy. The plastic   back ply prevents the passage of spall, in the form of projectile or glass fragments, while it dissipates the remaining kinetic energy.

(U)   The most efficient designs of transparent armor intended to defeat fragmentation from explosive ordnance have traditionally been monolithic or laminated plastic(s). Glass, due to its high density, is historically not competitive in defeating the irregularly shaped, and less-penetrating, fragment threats.

(U)   The state of the art in transparent armor has been unchanged for many years, due to the lack of higher-performance component materials such as transparent ceramics, glass / ceramics, glass, and plastics. No new plastic has been commercialized for use in the volume manufacture of transparent armor since polycarbonate was introduced into the market in 1958.

(U)   Simula Technologies, Inc., (Simula) is developing a new family of transparent polyurethane polymers which have an unusual combination of properties. Several of these polymers, even in their early stages of development, show great promise for improving the performance of many types of transparent armor.

(U)   Simula has recently performed several Government-funded research and development programs relating to transparent armor concepts for personal eye protection devices, helicopter armor, and the optimization of transparent armor designs using computational modeling. The results of this work show that it is now possible to create armor designs affording substantially higher protection or reduced weight by incorporating new, higher-performance transparent polymers.

(U)   **Background**

(U)   Simula's polymer development work was initiated as a company-funded research and development program which was conducted during 1993. At that time, Simula was performing the Helicopter Advanced Armor Concepts (HAAC) Program (Reference 1), for the U.S. Army Aviation and Troop Command, Aviation Applied Technology Directorate (AATD), Fort Eustis, Virginia. The purpose of this program was to develop and define weight-saving advanced armor concepts, both opaque and transparent, for helicopter applications.

(U)   Simula recognized the potential for improvements in the ballistic performance of transparent armor which could result from a polymer formulated specifically for armor usage. A program was begun to accomplish this task. Using newly available component materials and innovative chemistries, a family of new transparent polyurethane polymers was created. The first polymer of merit, S-1180, was incorporated into the final HAAC program blast / fragmentation barrier design samples delivered to the Government for testing. The Government-conducted live-fire testing using 23-mm high-explosive incendiary (HEI) ordnance demonstrated that the design offered the potential of meeting the program's ballistic performance goal at an areal density 20.4 pct lower than the program baseline in lieu of the   10 pct reduction program goal.

(U)   Simula's ongoing work has, to date, resulted in a family of thermoset and thermoplastic polymers which far exceed the properties and performance attained with S-1180. The identification codes, physical, mechanical, optical, and ballistic properties for the currently best-performing polymers will be presented later.

(U)   **New Polymer Properties**

(U)   The best-performing polymer developed and characterized to date is SIM 2003, which is also known as Cleargard™. The properties of SIM 2003 are shown in Table I. The properties of as-cast acrylic and polycarbonate are included for comparative purposes. The superior properties of the new polymer has expanded the scope of the materials' potential product applications well beyond the original program goals.

Table I. (U) Comparative polymers properties data				
Property	Units	As-Cast Acrylic	Polycarbonate	SIM 2003
Color	-	Water Clear	Water clear, Light gray, or Light straw	Near water clear
Yellowness Index	-	-	1.00	2.00
Specific Gravity	-	1.20	1.20	1.14
Hardness	D Scale	92-93	84-86	80-81
Fischer Microhardness	N/mm^2	184	116	62.6
Luminous Transmittance	Pct	91	89	93
Haze	Pct	1.0	0.6-1.0	0.5
Refractive Index	-	1.490	1.586	1.538
Abbe No.	-	-	27.0	40.0
Heat Deflection Temperature (254 $lb/in.^2$)	°F	212	276	300
Stress Craze Resistance (isopropyl alcohol)	$lb/in.^2$	3,800	4,000	>7,000
Tensile Strength - Ultimate	$lb/in.^2$	10,500	9,500	7,326
Elongation	Pct	4-5	80	286
Modulus	$lb/in.^2$	450,000	340,000	118,000

(U)   SIM 2003 has exceptional toughness combined with very attractive optical properties. As is shown in Figure 1, SIM 2003 provides substantially higher ballistic performance than polycarbonate or as-cast acrylic. These data were obtained using MIL-P-46593A fragment-simulating projectiles (FSP's). The

---

™ Cleargard is a trademark of Simula, Inc. (U)

family of MIL-P-46593A FSP's were developed by the Government for use as simulants for the fragments produced by various types of explosive ordnance (See Figure 2). Their use in laboratory ballistic testing facilitates the generation of comparative data for competing armor systems.

(U)   It is informative to note that 0.125-in.-thick SIM 2003 provides the same V_{50} PBL as does the 0.25-in.-thick polycarbonate. However, the polycarbonate data shown in Figure 1 is comparatively overstated for most eye protection devices. The data was obtained by testing polycarbonate in extruded sheet form, which has higher ballistic performance than the grades of polycarbonate which are injection-molded into optical devices such as visors and lenses.
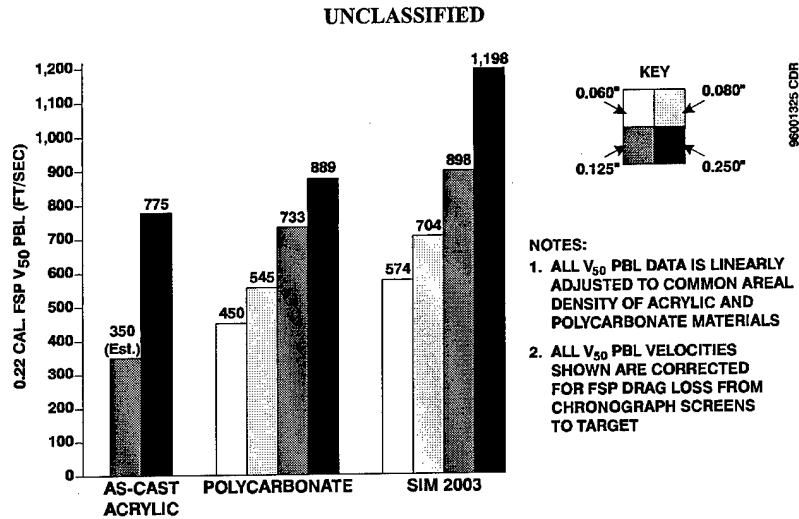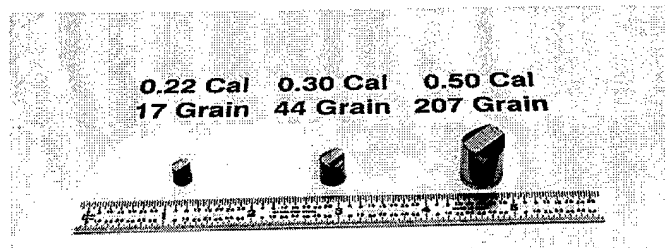
UNCLASSIFIED

Figure 1. (U) Comparative polymer ballistic test data.

UNCLASSIFIED

Figure 2. (U) Fragment-simulating projectiles per MIL-P-46593A.

UNCLASSIFIED

(U)   The SIM 2003 polymer's lack of color, high luminous transmittance, and very low haze characteristics support its use in critical optical applications such as helmet visors, face shields, goggle lenses, spectacle lenses, and aircraft transparencies. SIM 2003 has chemical resistance, abrasion resistance, and thermal resistance properties that far exceed those of polycarbonate. SIM 2003 also has a specific gravity of 1.14, which is 5.0 pct less than acrylic and polycarbonate, and 13.0 pct less than allyl diglycol carbonate.

(U)   The chemistry of SIM 2003 offers broad formulation freedom and very tailorable processing characteristics. These attributes facilitate adjusting properties to meet specific application requirements, and attaining an economical manufacturing process. The chemistry of SIM 2003 is compatible with many specialty additives such as melanin, which is a natural skin pigment now being employed as an advanced ultraviolet radiation blocker for eye protection.

(U)   <u>Simula Technologies' Polymer's Contributions to Advanced Armor Development Programs</u>

(U)   In addition to the previously mentioned HAAC program, Simula's new polymers have benefited several other advanced development programs in diverse fields as follows:

(U)   <u>Transparent Armor Technology Development Using Computational Modeling Program</u>

(U)   Simula performed the Transparent Armor Technology Development Using Computational Modeling Program for the Advanced Research Projects Agency (Reference 2). This program was technically monitored by the U.S. Army Tank Automotive Command, located in Warren, Michigan. Simula's work, supported by Sandia National Laboratories (SNL) and Los Alamos National Laboratory (LANL), further developed advanced shock physics codes during the analysis of state-of-the-art designs. The improved hydrocodes were then applied by SNL and LANL to create new lighter-weight armor designs. Simula's S-1180 and SIM 2003 polymers were included in the program, together with commercial glass and polycarbonate materials.

(U)   Simula's fabrication and ballistic testing of the model-generated designs showed the SNL CTH hydrocode modeling of both monolithic- and laminated-polymer-based designs to be highly predictive of the armor's empirical ballistic performance. The LANL modeling of the glass / plastic armor designs using their MESA2D and SPHINX hydrocodes to computationally predict the ballistic performance of new designs was less successful.

(U)   <u>Enhanced Dyes For Laser Eye Protection Program</u>

(U)   Simula's SIM 2003, and a highly cross-linked thermoset polyurethane, SIM 1802,were recently evaluated within the Anteon Corporation's Enhanced Dyes for Laser Eye Protection Program performed for the U.S. Air Force (Reference 3). The new polymers offer the ability to incorporate laser-absorptive dyes (both current-production and newly synthesized dyes) directly into a liquid component of the polymer prior to compounding. This solubility feature ensures homogeneity of the dye dispersal. The tailorability

of the polymer cure temperature enables the use of certain high-performance dyes that are normally destroyed by the high temperatures imposed during the injection molding of polycarbonate optical devices.

(U)   During the program, a total of 16 production dyes and 7 newly synthesized dyes were evaluated for compatibility and solubility with SIM 1802 and SIM 2003 polymers. Excellent results were achieved, with all 23 of the dyes being successfully incorporated into SIM 2003, and 13 of the dyes being incorporated into SIM 1802. Test coupons were delivered and optical density values were measured at each laser wavelength of interest. Much optical design work remains to be accomplished as part of a recently awarded follow-on program. Simula will work to optimize the concentration of individual dyes in the polymer host to achieve the required optical density. Subsequent work will incorporate a multi-dye recipe into the polymer which maximizes user visibility while blocking multiple wavelengths of laser radiation to an eye-safe level.

(U)   Advanced Lightweight Transparent Armor Program

        Simula was recently awarded the Advanced Lightweight Transparent Armor (ALTA) Development Program by the U.S. Army Aviation Applied Technology Directorate located in   Fort Eustis, Virginia (Reference 4). The ALTA program represents a major development effort to advance the state of the art for two categories of transparent armor: glass / plastic laminate windshield armor, and plastic laminate blast / fragmentation barrier armor. The ALTA program's technically challenging goal is to further reduce the areal density of both categories of armor by 35 percent beyond the 10-percent reduction achieved in the previously described HAAC program.

(U)   Simula's technical approach for the ALTA program leverages off of the higher-performing materials developed since the HAAC program ended. These improved materials come from Simula's internally funded polymer development programs, as well as from a number of outside company and academia sources identified during the conduct of the program's Task 1 - Literature Search and Armor Technology Survey.

(U)   Simula has prepared and prioritized initial armor system designs incorporating various combinations of the new materials for both categories of transparent armor. Component materials have been both procured and manufactured for the prioritized designs which are scheduled to undergo the first ballistic testing. Several of the initial candidate designs are shown in Figures 3 though 6.

(U)   Based upon the measured performance of the designs and the behavior of the materials contained within the designs, an iterative series of design changes to the architecture and component scaling will be determined, and then fabricated, and tested. Simula will seek to further improve the best-performing new component materials through reformulation activities conducted either in-house on Simula's polymers or conducted outside the company by the material manufacturers.

(U)   The ballistic performance of the competing armor system designs will be tested in Simula's DoD-certified ballistic test facility. Deliverable samples of the best-performing design will be subjected to ballistic testing at AATD's ballistic test facility. An optional ALTA task exists which, if exercised, would involve providing selected replica windows for the AH-64 Apache attack helicopter and the C-17 Globemaster III and C-130 Hercules fixed-wing aircraft. The replica windows would incorporate the lightest-weight transparent armor which meets or exceeds the program's weight-reduction goal. The

replica windshields would be non-flightworthy articles capable of undergoing testing and evaluation activities both on a stand-alone basis and after being installed on a representative aircraft.
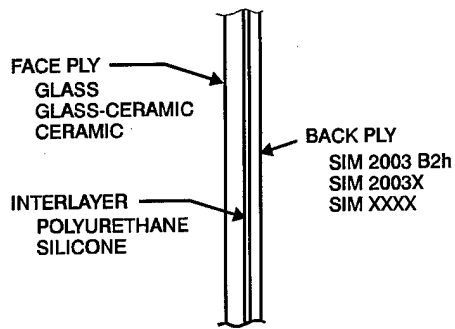
FACE PLY
GLASS
GLASS-CERAMIC
CERAMIC

BACK PLY
SIM 2003 B2h
SIM 2003X
SIM XXXX

INTERLAYER
POLYURETHANE
SILICONE

Figure 3. (U) Windshield armor.

FACE PLY
GLASS
GLASS-CERAMIC
CERAMIC

BACK PLY
SIM 2003 B2h
SIM 2003X
SIM XXXX

INTERLAYER
POLYURETHANE
SILICONE

INTERMEDIATE PLY
PARMAX™ 1200
SIM 102998
SIM 1803
SIM XXXX
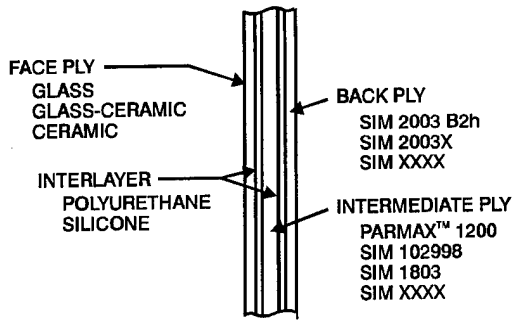
Figure 4. (U) Windshield armor.

SIM 2003 B2h
SIM 2003X
SIM XXXX
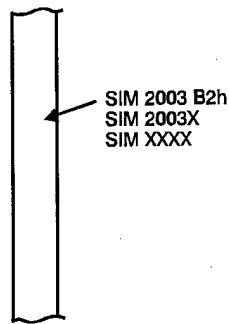
Figure 5. (U) Blast / fragmentation barrier.

FACE PLIES
SIM 2003 B2h
SIM 2003X
SIM XXXX

INTERLAYER
POLYURETHANE
SILICONE

INTERIOR PLIES
PARMAX 1200
SIM 102998
SIM 1803
SIM XXXX
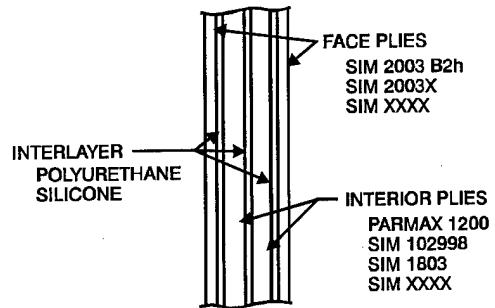
Figure 6. (U) Blast / fragmentation barrier.

™Parmax is a registered trademark of Maxdem, Inc. (U)

(U)   **Improved PASGT Helmet Visor Incorporating New Polymers**

(U)   The U.S. Army has expressed an interest in fielding a PASGT helmet visor which affords the same fragment protection level as the helmet body. The visors currently fielded are made of polycarbonate, and even the thickest designs fall far short of providing a 2,000-ft/sec V_{50} PBL performance against the 0.22-cal. FSP. Two new candidate visor designs for defeating the 2,000-ft/sec FSP threat are shown in Figure 7. The monolithic polymer design is preferred for simplicity, low cost, and optic quality; however, the dual-hardness design should be capable of providing the thinnest, lightest-weight possible visor capable of defeating the ballistic threat.
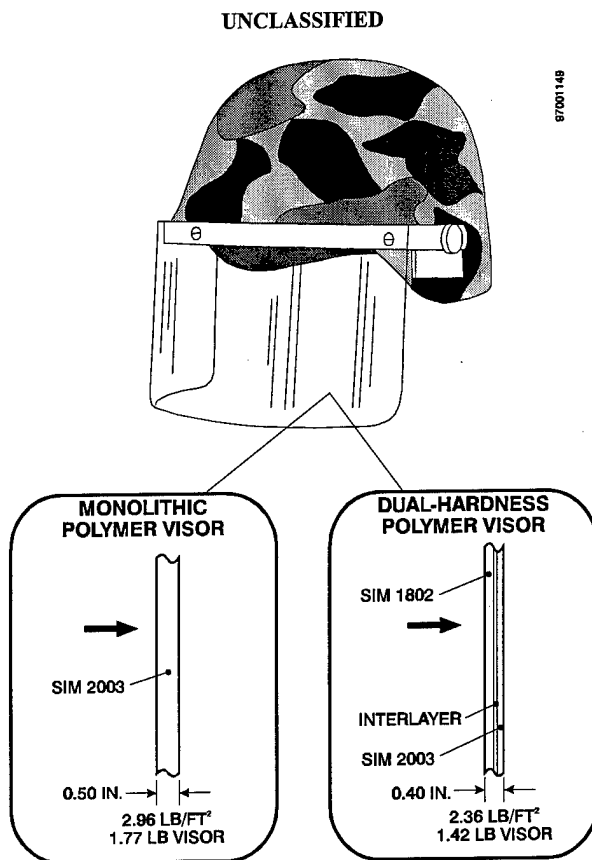
UNCLASSIFIED

Figure 7. (U) High-performance helmet visor designs.

UNCLASSIFIED

(U)   The new polymers are still in their development and scale-up phase, and further improvements in ballistic performance are anticipated by altering the soft-segment-versus-hard-segment of the polymer backbone, and/or by polymer alloying. These changes, if needed, combined with optimization of design architectures, offer great promise of meeting or exceeding the helmet visor weights shown in Figure 7.

(U)   The high-performance polymer(s), whether monolithic or laminated, will provide very important advantages for manufacturing low-cost and robust visors for military use. The monolithic-polymer visor design can be liquid-cast to shape or formed from a flat sheet. The dual-hardness polymer visor design can be formed from a laminated flat sheet. Both the cast-to-shape and forming processes will yield excellent optical quality. The all-polymer visors will be highly break-resistant in service. The monolithic-polymer visor design eliminates the potential for in-service delamination.

(U)   The optical surfaces of Simula's polymers will require a hard coating to provide a durable protective device such as a helmet visor for military use. However, the commercial hard coatings typically applied to polycarbonate work well with both the SIM 1802 and SIM 2003 polymers. Simula is also evaluating diamond-like coatings (DLC) on the new polymers to impart truly scratch-resistant protection.

(U)   Glass / plastic laminate visor designs will likely not be competitive in terms of weight, manufacturing cost, and durability. A visor made to fit the PASGT helmet requires a radius of curvature of approximately 4.5 inches. Matching the shape of the glass and plastic components within the very tight tolerances required for successful lamination and acceptable optics poses a major technical challenge. It is extremely difficult to consistently form glass to such a tight radius while maintaining unmarked surfaces.

(U)   A glass / plastic visor design imposes substantial risks of glass breakage and delamination. The relatively thin glass facing ply supported by a soft plastic interlayer is vulnerable to breakage due to impact with hard objects during manufacture and while in service. The delamination risk results from stress concentrations generated during lamination, residual stress in the finished laminate, and stress induced by temperature change due to the very dissimilar coefficients of thermal expansion of the glass and plastic components.

(U)   Acknowledgements

(U)   The author wishes to acknowledge the contributions made by the following Simula employees. Simula's polymer development work is performed under the direction of Dr. Paul Apen, the Manager of Advanced Materials Development. Edwin C. Slagel, Staff Chemist, created the S-1180, SIM 1802 and SIM 2003 transparent polymer formulations. Very significant contributions have also been made by Chemist Robert L. Fogarty in the refining and characterizing of the polymer formulations and processing techniques.

(U)   References

1. (U) Lyons, F. S., Huyett, R. A., and Hardtmann, D. J., "Helicopter Advanced Armor Concepts," USAATCOM TR-94-D-16, July 1994.

2. (U) Lyons, F. S., Huyett, R. A., Hertel, Jr., E. S., Henninger, R. J., and Mandell, D. A., "Transparent Armor Technology Development Using Computational Modeling," TR-94127, Simula Government Products, Inc., Phoenix, Arizona, August, 1994.

3. (U) Huyett, R. A., "Anteon Corporation Subcontract No. 96-5000-64-9, Enhanced Dyes for Laser Eye Protection," issued under U.S. Air Force, Wright Laboratory, Materials Directorate, Hardened Materials Branch, Contract No. 33615-92-D-5000, Delivery Order No. 64-9, Rev 1.

4. (U) Contract No. DAAH10-98-C-0031, "Advanced Lightweight Transparent Armor", issued by the U.S. Army Aviation Applied Technology Directorate, Fort Eustis, Virginia.

(U)   Author Biography

(U)   Richard A. Huyett
        Simula Technologies, Inc.
        10016 South 51st Street
        Phoenix, AZ 85044
        Phone: 602-753-2099
        Fax: 602-893-8643

(U)   Mr. Richard A. Huyett holds an A.A. Degree in Mechanical Design Technology from Southern Illinois University. As a Senior Project Engineer at Simula Technologies, Inc., he conducts R&D of transparent armors including transparent polymers for protective applications. He performs mechanical, optical, and ballistic testing and evaluation on new transparent products. He is the Principal Investigator on three Simula Technologies internal R&D programs that are developing transparent polyurethane polymers. Mr. Huyett has also acted as Project Engineer on numerous Government-sponsored R&D programs relating to transparencies.

(U)   Prior to joining Simula Technologies, Mr. Huyett worked at Loral Defense Systems, Arizona Division (formerly Goodyear Aerospace Corporation) as a Section Head of Transparent Products Engineering. He has 29 years of experience in the fields of transparent armor and aircraft transparencies, and has authored numerous technical reports and papers.

PERFORMANCE TESTING OF THE AN/VVR-1 LASER WARNING RECEIVER

Glenn J. Benecke
Raytheon Systems Company
Danbury, CT 06810

ABSTRACT (U)

(U)   The AN/VVR-1 Laser Warning Receiver, developed by Raytheon Systems Company, is currently under evaluation by the U.S. Army. The AN/VVR-1 uses a Fabry-Perot etalon to detect laser radiation, a Gray Code for Angle-of Arrival (AOA) determination, and signal processing techniques to identify laser beamrider missiles.   In October 1997, the system completed performance testing at the Naval Air Weapons Center in Lakehurst, NJ. The ability of the system to detect laser events exceeded a 95% Probability of Detection for rangefinders and designators with zero false alarms. The beamrider detection channel met its sensitivity requirements. The system has displayed the ability to determine the Angle of Arrival to a rangefinder or designator source to within +/- 0.8°. The system also correctly performed reflection processing, multiple threat detection, and threat tracking.

(U)   1. Introduction

(U) In 1996, Raytheon Systems Company, formerly Hughes Danbury Optical Systems, built two prototype Laser Warning Receivers (LWRs) utilizing state of the art component technologies that Raytheon had developed under an IR&D program. These IR&D efforts included:

- Application Specific Integrated Circuits (ASICs) to reduce sensor size requirements
  - Germanium Coherency and Angle of Arrival (AOA) detectors to extend the wavelength spectrum to include eye-safe lasers in a single detector
  - Improvements in AOA resolution
  - Data interfaces for both bused (MIL-STD-1553B) and non-bused (RS-422) vehicles
  - Improvements in processing algorithms

(U) These two Raytheon K17 series LWRs (Figure 1) were designed to meet the requirements of ground vehicles. The K17A was a single package design providing a Field of View (FOV) of 360° in azimuth and ±55° in elevation. The system had single

axis AOA detection capability in the front quadrant and a built in system processor. The K17W integrated the same technologies into four separate sensor units, each with a FOV of ±55° in azimuth and elevation and single axis AOA detection.
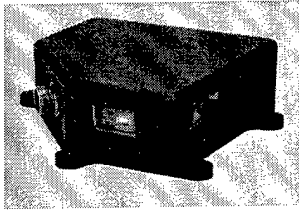
K-17A   K-17W

Figure 1. K-17 Laser Warning Receivers

(U) The K-17W formed the baseline design for the AN/VVR-1. In 1996, CECOM contracted with Raytheon Systems Company for the delivery of the first AN/VVR-1 prototype systems. The AN/VVR-1 is currently completing this evaluation phase and is scheduled for a User Evaluation (UE) in August 1999 on the M2A3 Bradley.

(U) The AN/VVR-1 has completed system level performance evaluations to ensure the system meets the technical specification required by the US Army. The primary evaluation of the AN/VVR-1 occurred in October 1996 at the Naval Air Weapons Center at Lakehurst, NJ.

(U)   2. <u>AN/VVR-1 System Description</u>

(U)   <u>Coherency Detection</u>

(U) During Raytheon's initial work in laser detection, we decided to develop a LWR using a patented Fabry-Perot etalon. This provides both a high Probability of Detection (POD) and low false alarm rate. The etalon utilizes the coherence property of a laser to discriminate incoherent sources. By using coherence to sort laser radiation from other optical sources, we have achieved false alarm rates of less than 0.01/hour while maintaining high probability of detection for single pulse rangefinder threats.

(U) The etalon modulates the intensity of the light that is transmitted through it. This intensity modulation results from interference effects that occur with coherent light but not with non-coherent light. The coherent laser light will either constructively or destructively interfere as it passes through the etalon. This interference will change the intensity of the light from its nominal value to a reduced value for destructive interference and to an increased value for constructive interference. Non-coherent (non-laser) light will not interfere as it passes through the etalon, resulting in no

modulation. The result is a laser warning detector that provides a high Probability of Detection, very low false alarm rate, and wide dynamic range. The performance of this architecture has been proven in field trials and demonstrations worldwide.
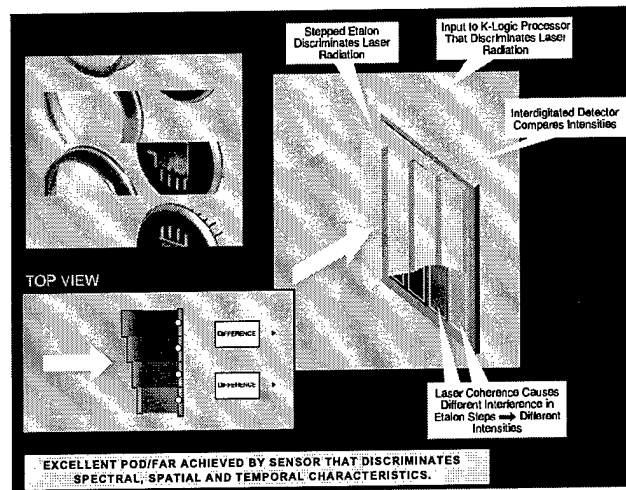
Figure 2. Raytheon Etalon Architecture

(U)   Angle of Arrival

(U) Raytheon has evolved an approach to AOA detection over many years of development and field trials. A single cycle of the Raytheon Gray code detector is shown below. A narrow slit mask over the detector creates a line image on the detector array from the laser sources. The location of the image is transformed to a unique (orthogonal to slit) angle in object space. Four cycles are reproduced on a single detector to eliminate noise in the angle of arrival due to atmospheric fluctuations that change the apparent location of the beam. For each angular location an n-bit digital word is formed with each bit corresponding to a particular row in one cycle of the detector. This approach has been demonstrated to be most robust to signal strength variations in the field.
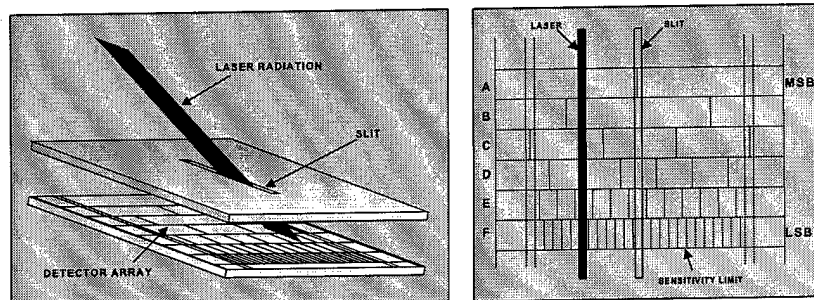
Figure 3. Raytheon Gray Code

(U)   <u>Laser Beamrider Missiles</u>

(U) Because of their unique guidance systems, laser beamrider missiles represent a challenge for detection. The beamrider missile receives its guidance beam from the missile launcher which transmits a set of coded laser signals to a receiver on the back of the missile. These signals are very low power since the laser energy is not reflected off a surface as in a rangefinder or designator. Also, the beam initially has a very large divergence that decreases as the missile travels down range. The beamrider signals are typically less than 0.1 % of the typical rangefinder designator signals detected by the LWR.

(U) The LWR must be capable of detecting this weak signal at missile launch to provide sufficient reaction time. Raytheon has developed the technology for detecting and recognizing these low level signals. Our detection techniques are based upon unique methods of signal detection and processing. These include the ability to minimize solar noise backgrounds, real time threshold monitoring, and sophisticated signal extraction processing. The system contains two high sensitivity, and parallel processing channels, for detection of laser beamrider threats. Each processing channel is optimized for the temporal characteristics of the two types of beamriders (high rep rate, short pulse width and high rep rate, chopped CW). Detection of the low-level signals used at launch to guide beamriding missiles has been proven many times in U.S. government field tests.

(U)   <u>System Architecture</u>

(U) The AN/VVR-1 consists of 4 sensor units (SUs) and an Interface Unit (IFU). The four SUs ensure full coverage in azimuth around the vehicle and allow for easier platform integration due to the overlapping fields of view.
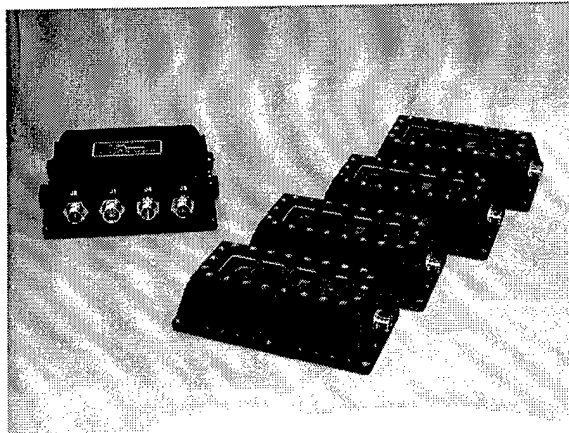
Figure 4. AN/VVR-1 System

(U) Each AN/VVR-1 Sensor Unit (SU) contains four detection apertures. Three of the apertures are used for the detection and AOA location (azimuth and elevation) of rangefinders and designators. The fourth aperture is used for detection of laser beamrider weapons.
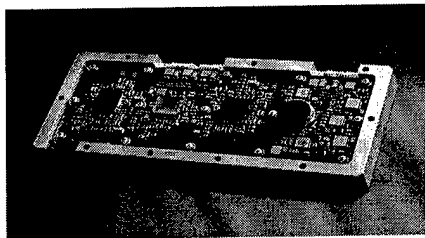
Figure 5. Detection Channels

(U) The AN/VVR-1 IFU serves as the LWR system processor and the interface to the vehicle for data transfer and system power. Upon detection of a laser event, threat messages are transmitted from the detecting SU(s) to the IFU via an RS-422 link. A single IFU can accommodate up to eight SUs. The IFU performs all system level processing functions including threat sorting and tracking, threat classification and AOA coordinate transformations from SU space to earth or vehicle coordinates. Two data I/O interfaces to the host vehicle are available: MIL-STD-1553B for bused applications and RS-422 for non-bused applications. The IFU also contains spare discrete and RS-422 I/O ports for individual user defined functions such as interface to laser countermeasure systems, IFF systems or laser communications systems. System software and user defined parameters such as threat classification parameters are modifiable via either an RS-422 port or the MIL-STD 1553B bus.

(U)   3. <u>System Performance Evaluation</u>

(U) During October and November 1997, the first AN/VVR-1 prototype was tested at the Naval Air Warfare Center (NAWC), Lakehurst, NJ. The objective of the test was to ensure that the AN/VVR-1 met the following performance requirements.

- Detect both 1.06 micron and 1.54 micron single pulse laser rangefinders with greater than a 95% PoD

- Do not detect threats targeted more than 15 meters from the platform. This has been achieved by customizing the sensitivity for a sharp roll off in detection at the prescribed 15m missed distance.

- No more than 1 false alarm per 24 hour period

- Provide azimuth and elevation to rangefinder and designator threats to within ±2°

- Identify the incident laser energy as either a beamrider, designator, or rangefinder

- Provide multiple target detection of 3 threats not separated by less than 10°.

- Does not report reflected energy as a threat

(U)   <u>Test Scenario</u>

(U) Testing was performed on Test Track 2, which provided a range of approximately 2.5km from the laser threat simulators (LTS) to the LWR site. The laser threats that were utilized were a 1.06 µm and 1.57µm laser operated at a 10Hz rep rate. There were two laser beamrider simulators available, an Airborne Laser Beamrider simulator and a Ground Laser Beamrider simulator.

(U) Tests were performed with the AN/VVR-1 system configured in two ways:

• Sensor tests - Sensors were mounted to get maximum sensor exposure to each laser pulse (i.e. 4 sensors at once). Test conducted in this configuration were for AOA accuracy, Probability of Detection vs. Offset Aimpoint (miss distance) and False alarm rates.

• System level tests - Configuration representative of the tactical deployment with mounting angles as expected in the final vehicle mounts, i.e. 90° with respect to each other. Tests conducted in this configuration were Laser reflection processing, sensor to sensor hand-off, AOA tracking vs. turret movement and multiple source reporting.

(U) For both of these series of tests the sensor mount was capable of rotation about both the azimuth and elevation axis. The rotary table and holding fixture used

precision two axis stepper motor drive and shaft encoders under computer control to move the sensors through both azimuth and elevation in a calibrated manner. The angle of rotation in both azimuth and elevation was recorded over a field of 120° and to an accuracy of 0.01°.

(U)   Data Collection

(U) The configuration of the sensor level tests allowed for 400 measurements for each data point. This was possible since the Laser Threat Simulator (LTS) fired 100 pulses at the four sensors. The sensors were rotated in azimuth 120° in 5° increments and they were rotated in elevation 100° in 10° increments. For example, one data point may be a missed distance of 10 ft, the azimuth to the laser of +15° and the elevation to the laser of -20°. The POD for each data point is the number of pulses detected divided by 400 total pulses multiplied by 100.

	Range	Increments	Number of Data Points
Azimuth	+60° to -60°	5°	15
Elevation	+50° to -50°	10°	11
Missed Distance	0 ft to 50 ft	5 ft	11

(U) The POD at a specific missed distance is the average of all PODs at that aimpoint. The missed distance was varied from 0 ft to 50 ft in 5 ft increments.
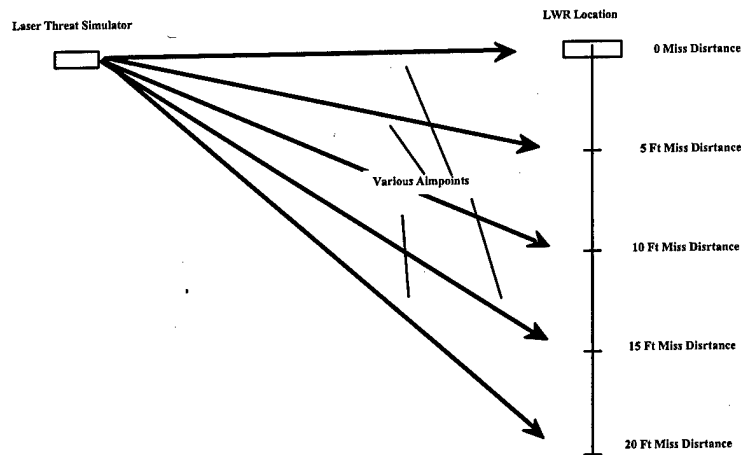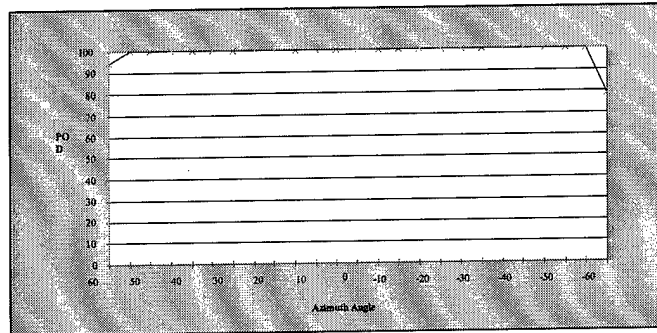

Figure 6. Miss Distance Layout

UNCLASSIFIED

(U)   Probability of Detection

        (U) The system achieved a 100% POD at the zero missed distance location.
Figure 8 below shows the POD for 0° elevation.

**Figure 7. Coherency Probability of detection at 0 foot miss distance, 0 degree
elevation**

(U)   Threshold

        (U) One of the specified requirements for any LWR is the detection capabilities
for an off-axis laser. In other words, how great a missed distance is desired? A large
missed distance may not be beneficial if the LWR is detecting lasers aimed at another
vehicle. The requirement for the Bradley installation is for the sensitivity to decrease
beyond 30 ft. For test purposes, a 50% POD at a 35ft. missed distance was required.

        (U) From previous K-17 field tests, Raytheon measured the Probability of
Detection (POD) of the coherence channels for both the 1.06μm rangefinder and
designator simulators to be >80% over the FOV at the maximum measurable miss
distance of 70 feet. Measurements beyond 70 feet could not be made due to obscurations
between the laser line-of-sight.
        (U) The thresholds on the AN/VVR-1 were adjusted to provide the optimal
sensitivity and missed distance capabilities. Figure 9 shows how the POD varied vs.
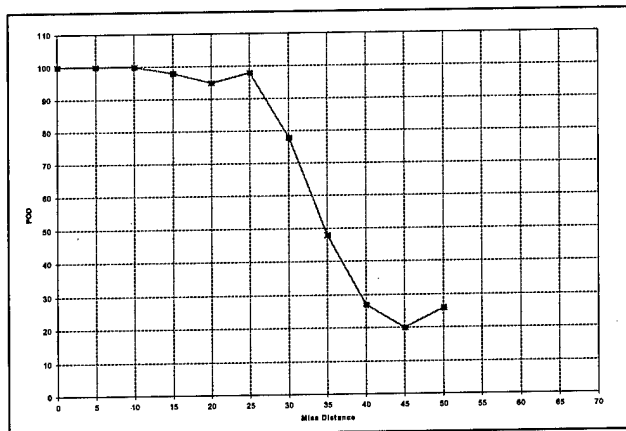missed distance.

UNCLASSIFIED

Figure 9. POD as a Function of Missed Distance

(U)   Angle of Arrival

Tests of AOA accuracy show that the system meets accuracy requirement of ±2°.
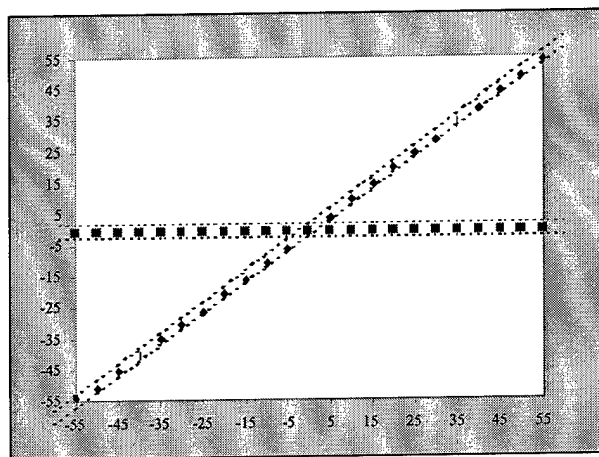Average errors of <0.8° were measured.

Figure 10. Reported Angle of Arrival for Zero Degrees Elevation

034

(U) Laser Beamrider Detection

(U) The sensitivity of the laser beamrider detection channel was measured meet the design objectives. The system provided the sensitivity required for exceptional performance against these types of threats.

(U) False Alarm Susceptibility

(U) Tests of false alarm susceptibility of the AN/VVR-1 included tests with the four sensors pointed directly at the sun for an extended period of time, a strobe light and simulated sun glint reflected into the aperture of the sensors. No false alarms were noted during any of the tests.

(U) Reflection Testing

(U) Reflection rejection algorithms were evaluated by the use of target mounted at the same range or slightly greater/lesser range to the sensors and making the target the aimpoint of the laser as shown in Figure A-6. The reflected energy from the target was directed into the sensor systems under evaluation to determine the capabilities of the reflection rejection algorithms in the system under test.

Laser Line of Sight

Target Board Locations
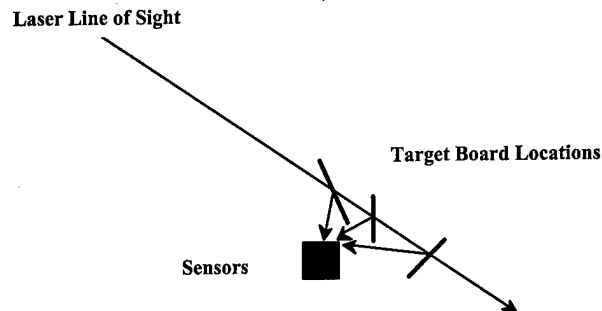
Sensors

Figure 11. Reflection Test Outline

(U) Reflection testing demonstrated that the AN/VVR-1 can discriminate between the main beam and reflections that occur with a 50 foot path difference, which was the design limit of the system. Since this test, system improvements have allowed for a 10m separation between the reflecting surface and sensor.
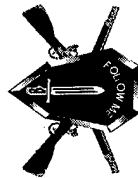
(U) Multiple Threat Detection

(U) The ability of the system to detect and output the correct laser threat AOA as the system is rotated through its complete field of regard (360° x 110°) was evaluated. This included the ability to correctly determine the AOA when the threat laser illuminates more than one sensor (overlap region). The system was able to report three separate threats illuminating a single sensor. Additional tests were performed that demonstrated correct tracking and reporting threats illuminating the same or separate sensors.

(U)   Conclusion

(U) The AN/VVR-1 has incorporated numerous Raytheon initiatives to reduce size, weight, and cost while increasing overall system performance. The system has been tested by the US government and has been shown to have a high Probability of Detection, low false alarm rate, enhanced laser beamrider detection capabilities, and high accuracy AOA capabilities. Additionally, the system has met its requirements for multiple threat reporting and rejecting reflected laser energy. In summary, the testing of the AN/VVR-1 at Lakehurst, NJ has demonstrated that it meets its specification and requirements.

Laser Warning Receiver System (LWRS)
User Interface (UI) Simulation Results

PM-GSI GROUND SYSTEMS INTEGRATION

United Defense

OptiMetrics

31 March 1999

Presented to:

10th Annual U.S. Army
Ground Vehicle Survivability Symposium

Presented by:

Jeffery V. Mosley
mosley@omi.com
(734) 973-1177 ext. 204
(734) 973-1199 (fax)

In Coordination with
PM-GSI, TSM-Bradley,
PM-BFVS, and UDLP.

Laser Warning Receiver System (LWRS)
User Interface (UI) Simulation Results

31 March 1999

Presented to:

10th Annual U.S. Army
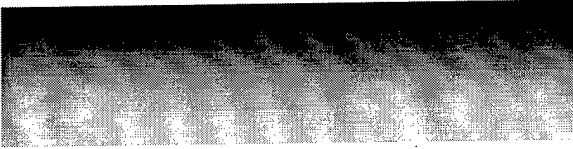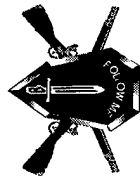Ground Vehicle Survivability Symposium

Presented by:

Jeffery V. Mosley
mosley@omi.com
(734) 973-1177 ext. 204
(734) 973-1199 (fax)

In Coordination with
PM-GSI, TSM-Bradley,
PM-BFVS, and UDLP

United Defense

OptiMetrics

Outline

- LWRS Overview
- UI Process
  - BPS/BPS Upgrade
  - Scenarios
  - User Survey
- UI Results Summary
- UI Lessons Learned and LWRS Path Forward

OptiMetrics, Inc.

AN/VVR-1 Laser Warning Receiver - Overview

Sensor
Units

Interface control
Unit (IFU)
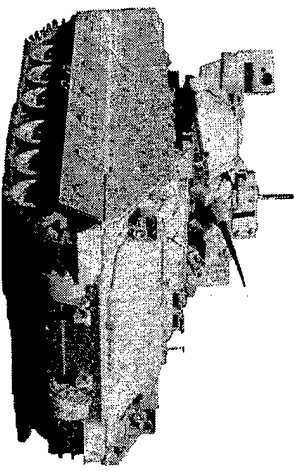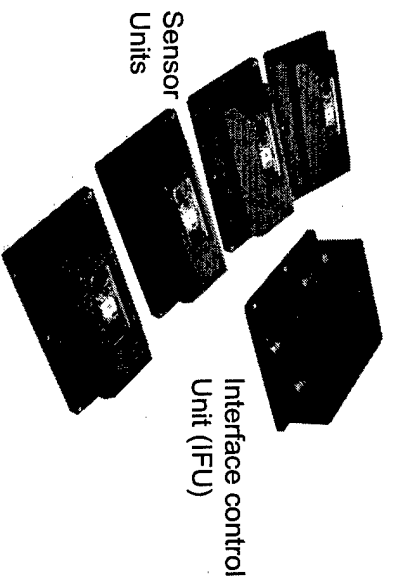
Planned integration in Bradley A3 FY99 developmental test. Awaiting
production dollars for A3 production cut-in as an ECP.

SYSTEM DESCRIPTION

The intent of a laser warning device is to alert the LWR
equipped crew they are being lased by a laser range finder,
designator or laser guided weapon. Laser receptors are
placed on the system and integrated via a Commander's
Decision Aid processor. Once lased, crews can be
provided a visual and audible warning as well as the back
azimuth to the lasing source, thus increasing their ability to
influence a pending enemy strike. The laser warning is an
HTI program leveraging aviation technology. The first
system to integrate the device will be the Bradley A3.

EMERGING INSIGHTS

- Modeling indicates a potential 30% reduction in
  soldier and vehicle casualties.
- Previous soldier in the loop simulations on a
  Bradley A3 simulator demonstrate a reduction in
  enemy target acquisition time from an average of
  27.1 seconds to 4.2 seconds.
- System participated in AWE 94-7 with positive
  soldier feedback.
- Technology is low risk.

OptiMetrics,
Inc.

Laser Warning Receiver (LWR)
How It Works

Threat Laser Sources

Designator

Beam Rider

Rangefinder

Laser Warning Receiver

LWR
Aperture

Internal
detectors and
software

Electrical
Connector
('Links LWR to IFV
and databus)
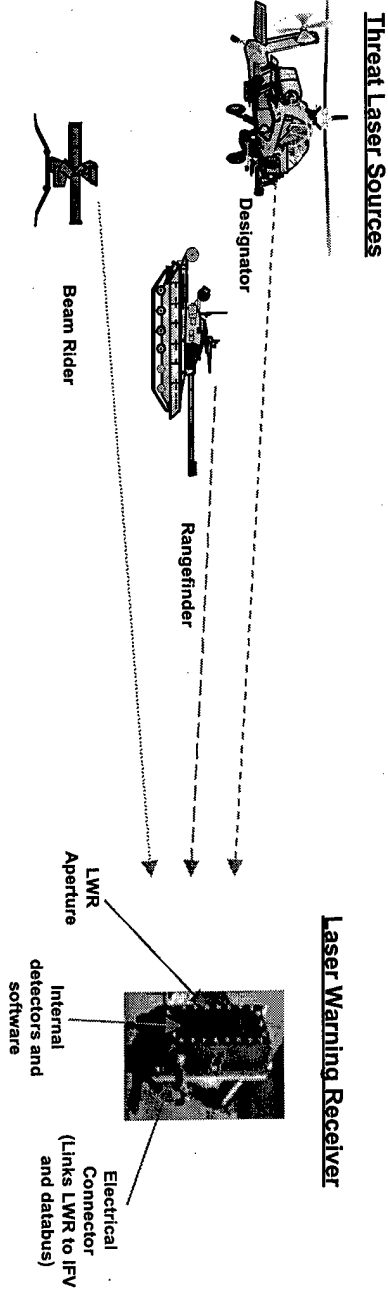
- Threat activates/employs laser (rangefinder, designator, or beamrider)
- Laser energy passes through atmosphere, hits LWR, passes through LWR aperture, hits internal detectors
- Detectors produce electrical signal, LWR software processes signal, declares laser event and classifies threat
  laser as rangefinder, designator, or beam rider
- LWR sends laser alert to Bradley databus, databus carries info to Turret Processor Unit (TPU)
- Turret Processor Unit (TPU) directs activation of laser alert signals for Bradley crew:
  – Audio alert over intercom system
  – Graphic/video alert on Biocular Display and IBAS

OptiMetrics,
Inc.

041

LWRS/SSES SW/HW Functions for Bradley A3

OptiMetrics, Inc.

D:\powerpnt\vg\vg-146.ppt(03/31/99)mnt Slide #5
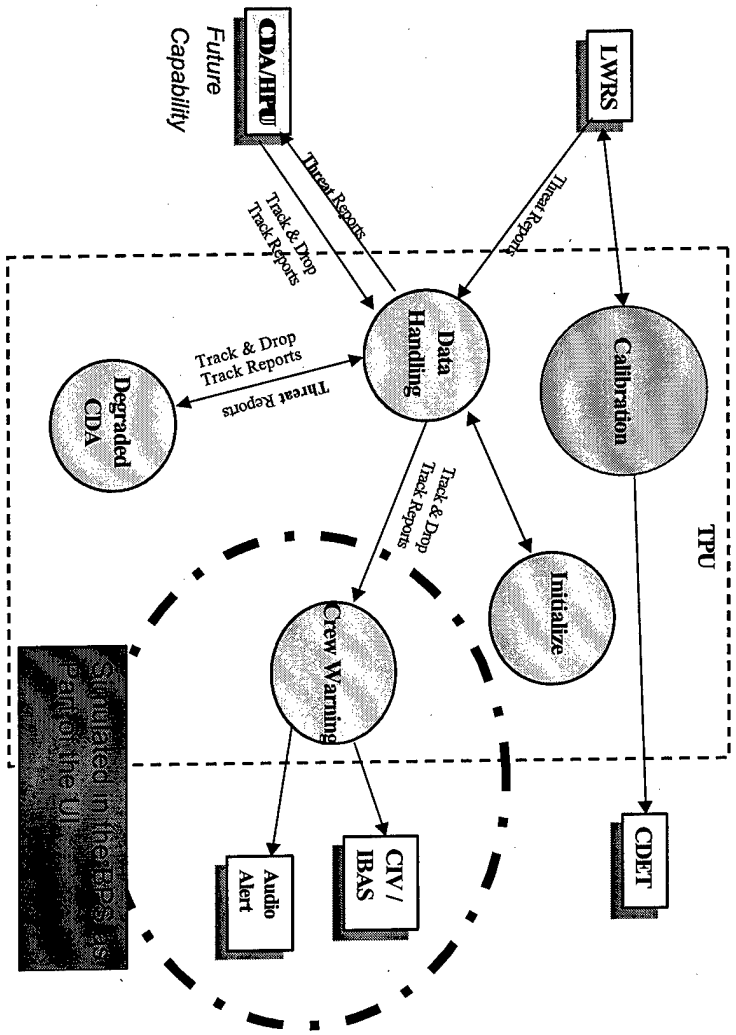
UI Process

A User Jury was conducted on 30 June and 1 July to validate the user interface planned for the SSES on the A3. The TSM-Bradley soldiers for the Evaluation Jury were:

> SFC William S. Grant
> SFC Ron Kuykendall
> SFC George Moore
> SFC Billy Smith

The tests were conducted as if there were four crews made up of the Jury members. Each Crew consisted of a Gunner and Commander.

The jury members traded seats so that each person acted in the capacity of gunner and commander. The interactive driver function (third crewman) was not available, although a simulated driver function was added to facilitate movement to contact, turning, and stopping for offensive scenarios.

Of particular interest were the implementation of Audio sounds and use of the CIV slew capability. Approximately 16 individual scenario runs were executed for each of the four crews.

OptiMetrics, Inc.

Bradley Plus Simulator

- Description - The BPS as part of UDLP's Combat Simulation and Integration Lab (CSIL) and Crew Station Module (CDM) support soldier in the loop virtual simulation for Bradley A3.

- BPS Upgrades - BPS required upgrade to support the UI included modeling of:
  - Laser sources (LRF, LTD, and LBR)
  - Crew Visual Displays (CIV/IBAS TPI)
  - Crew Audio Warnings (Tone, AoA, Laser Type, Repetition, and Age-out)
  - Crew Actions/Responses (i.e., CIV Slew, Target Hand-off)

- UDLP Support - UDLP as the LWRS and A3 system integrator provided highly professional engineering, programming, and technical support to the UI execution.

OptiMetrics, Inc.

Familiarization Task Scenario
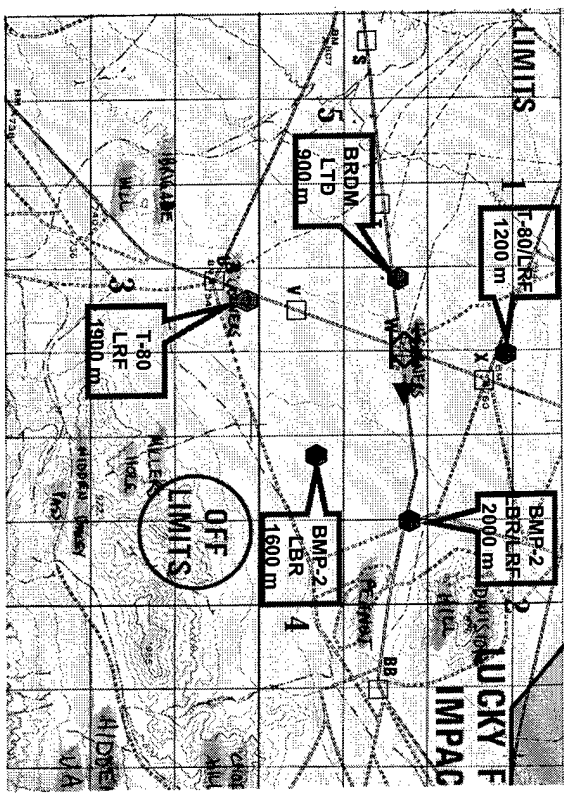
Simulation Objective - Provides BPS crews hands-on training so that they may become familiar with LWRS specific controls, functions, and TPI symbology.

OptiMetrics, Inc.

045

Audio Task Scenario
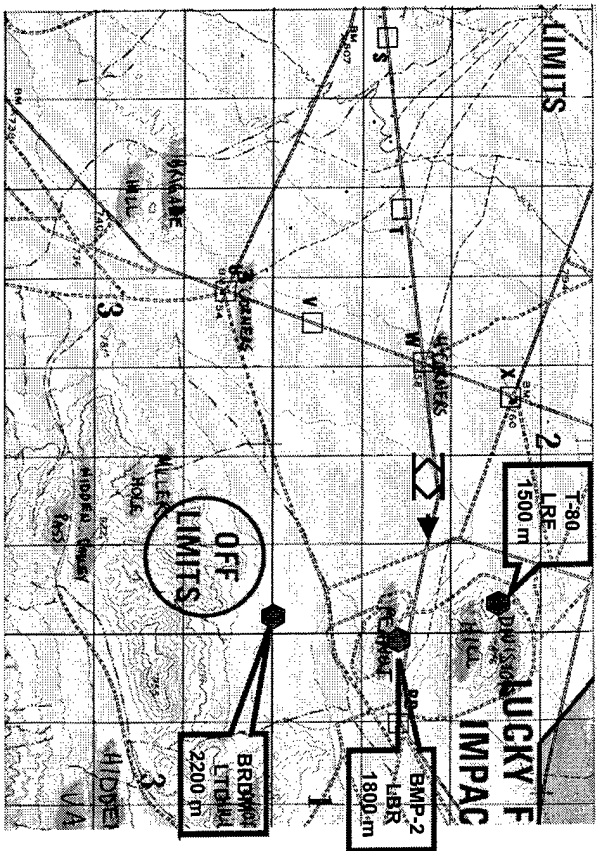
Simulation Objective - To present BPS crews with alternative audio and tone warnings. The crews will select a warning/tone type that will be used in the engagement scenarios.

OptiMetrics,
Inc.

Defensive Task Scenario
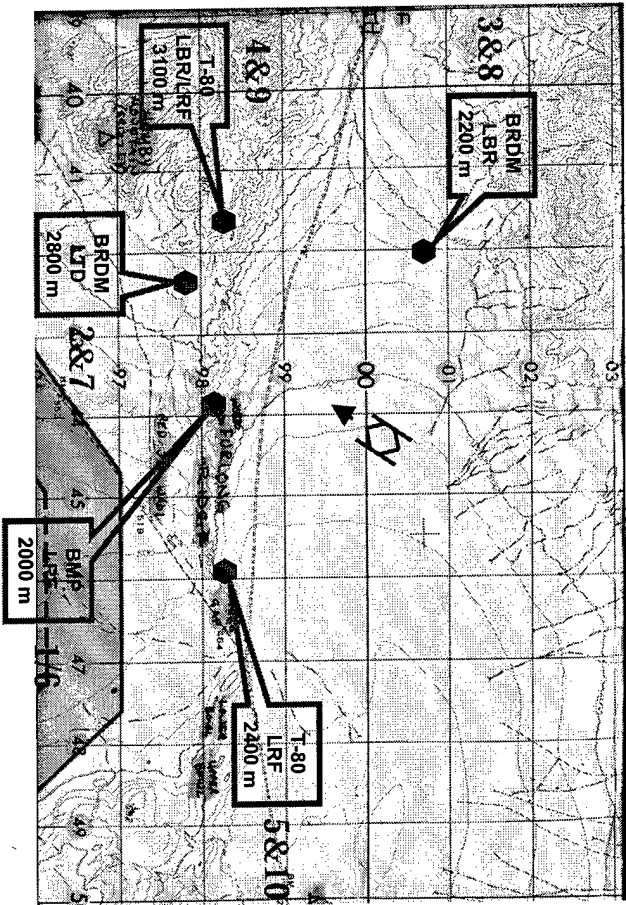
Simulation Objective - To provide BPS crews with threat scenes for defensive (static) interactive laser threat engagement. The vehicle will be simulated as being out in the open.

OptiMetrics, Inc.

Offensive Tasks
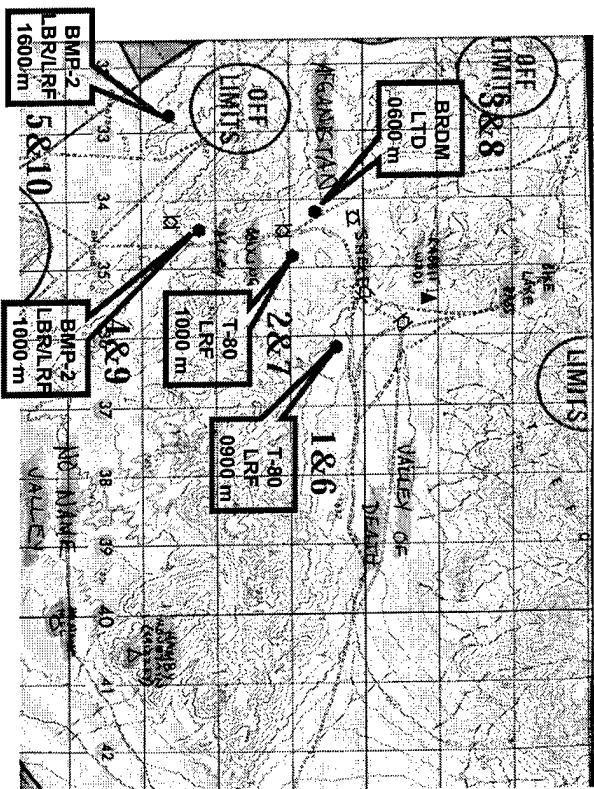
Simulation Objective - To provide BPS crews with threat scenes for offensive (moving) interactive laser threat engagement. Routes and waypoints were pre-determined. No maneuver CM was used.

———— OptiMetrics, Inc.

UI Survey

Questions were designed to collect data on the following areas:

- Audio Alert
- Visual Alert
- LWRS Contribution in Offensive/Defensive Maneuver
- Test Program Effectiveness

The results show general acceptance of the planned SSES approach. The jury seemed to be very impressed with the proposed capability and with the testing and simulation capability of the Bradley Plus Simulator.

Jury supported LWRS functional design changes were:

- An alert sound and format was selected.
- The CIV slew capability was changed to operate when the detected threat was a beamrider.

OptiMetrics, Inc.

Summary of Results

Target	Bradley With LWRS		Bradley Without LWRS	
	Acquisition Time From Threat Target in Sight = A (Seconds)	Acquisition Time From Threat Laser Fired = L (Seconds)	Acquisition Time From Threat Laser A (Seconds)	Acquisition Time From Threat Target in Sight = A (Seconds)
LRF	3.90	2.00	24.30	
LTD	3.90	2.20	34.80	
LRF/LBR	4.90	2.80	22.20	
LBR	18.90	13.20	25.00	

Timeline Without LWRS

T=0   T=A

Timeline With LWRS

T=0   T=L   T=A

T=0
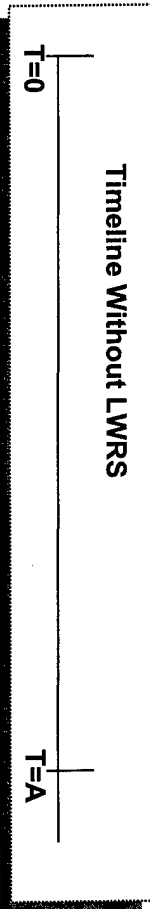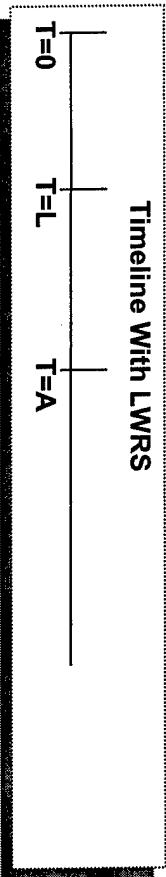
T = 0 - Time When Threat Target Appears in the Line of Sight
T = L - Time When the Threat Laser is Fired
T = A - Time When Crew Acquires the Target

OptiMetrics, Inc.

Initial Summary of Results

(LWRS in Bradley Plus Simulator)

Seconds

40
35
30
25
20
15
10
5
0

BRDM with Target Designator

BMP-2 with Laser Beamrider with Rangefinder

BMP-2 with Laser Beamrider without Rangefinder

T-80 Tank with Rangefinder

- Bradley without LWRS
- Bradley with LWRS
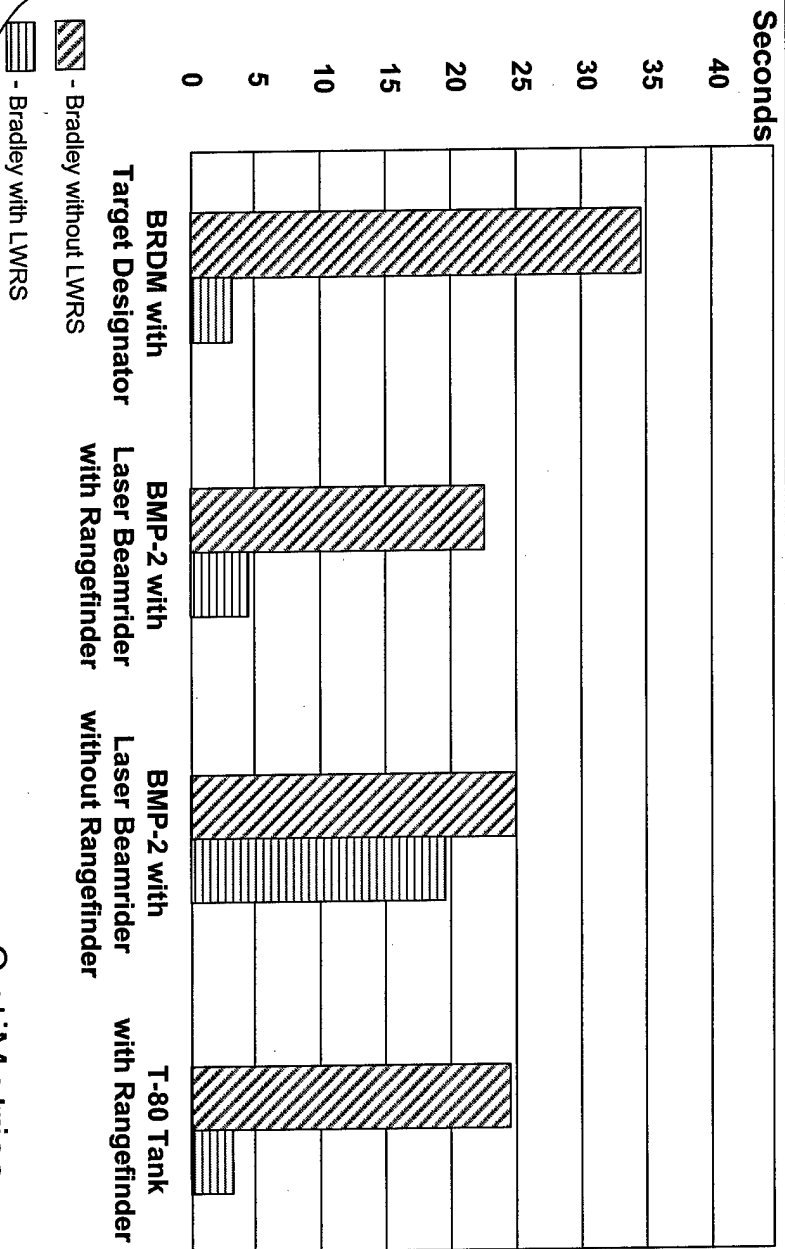
OptiMetrics, Inc.

A3 - SSES System Definition

Sensor Units

INU

LWR System

Detects laser energy

Interface Control Unit (IFU)

Attitude Data

Threat Reports

TPU

Biocular Display

IBAS Display

Audio Warning
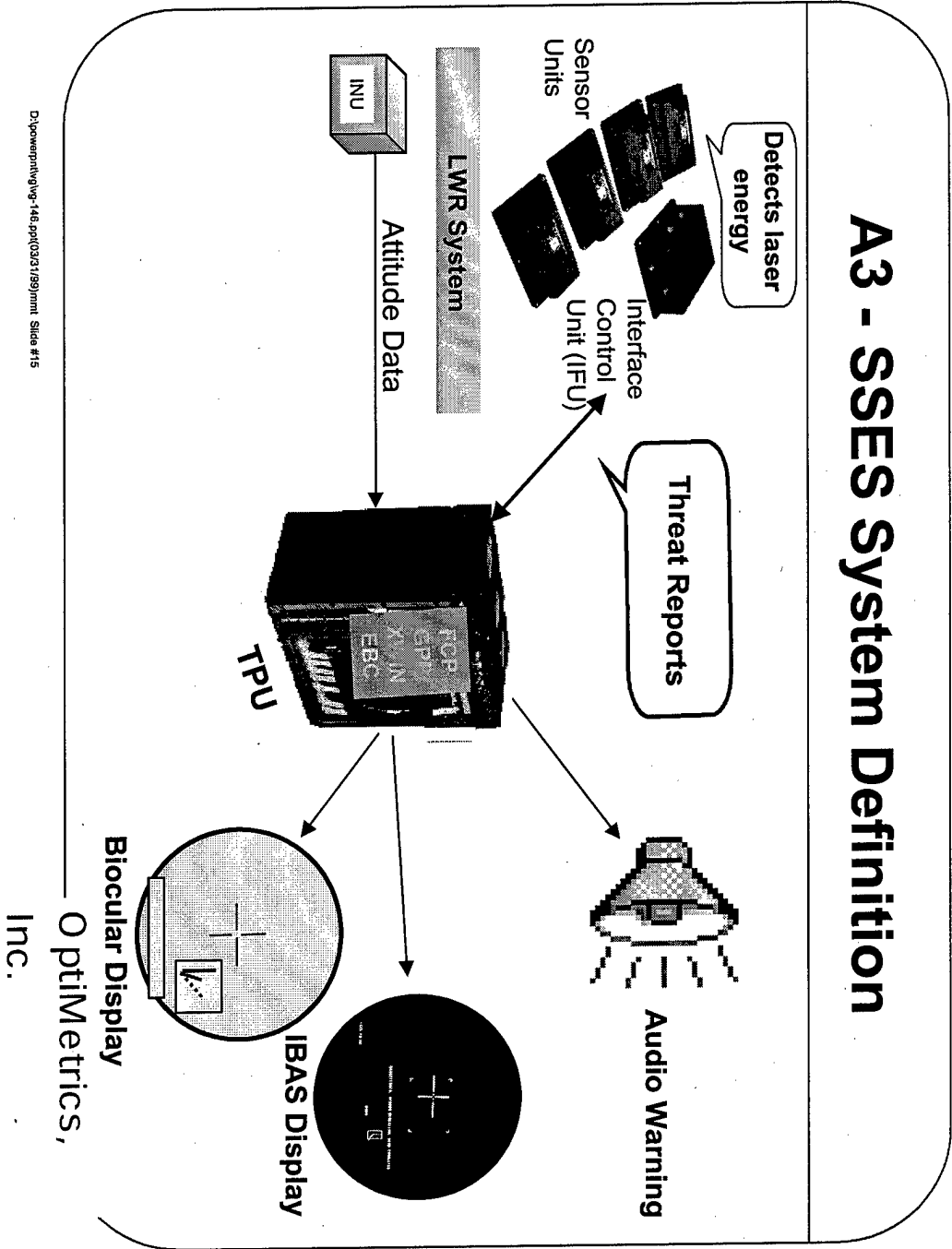
OptiMetrics, Inc.

LWRS UI Simulation Lessons Learned and Path Forward

- Lessons Learned - The development of the simulation with User input created a near real-time interactive design environment for the LWRS interface. The use of simulation for SMI and TTP development promotes efficient use of program resources.

  The User is very adaptive when given value added information such as laser threat AoA. The BPS Commander and Gunner effectively demonstrated the hunter/killer vehicle concept during the simulation.

- LWRS Path Forward - LWRS is currently integrated on the UDLP facilities vehicle. Leveraged technical testing with the A3 will be executed in the spring. The UI scenarios will be re-used in the summer as part of the LWRS User Evaluation (UE).

OptiMetrics, Inc.

Simulation Supported Acquisition:
An Examination of Metrics, Processes, and Integration

Dr. Paul H. Deitz, Technical Director

US Army Materiel Systems Analysis Activity

ATTN: AMXSY-TD

Aberdeen Proving Ground, MD 21005-5071

DSN 298-6598, (410) 278-6598, phd@arl.mil

1 April 1999

Presented at the 10th Annual U.S. Army Ground Vehicle Survivability Symposium, held at the U.S. Naval Postgraduate School, Monterey, CA, March 30 - April 1, 1999.

AMSAA

/vld/phd/ndia/gvss.99/vgs/g10

054

OUTLINE

- New Operational Challenges
- Extending the V/L Taxonomy
- The Ballistic Live-Fire Process
- Generalizing the Live-Fire Operator
- Levels/Operators/Military Operations Context
- The Fourth Dimension
- Mission-Based Acquisition Strategy
- Summary & Conclusions

055

New Operational Challenges

- Emphasis away from missions with massed forces

→ Loss Exchange Ratios no longer primary figure of merit

- New Operational Challenges:
  - Smaller/lighter forces
  - High Lethality
  - Situational awareness
  - Rapid deployment
  - Extended (self) sustainment
  - Emphasis on crew/platform survivability
  - Night/stealth missions
  - Improved effectiveness via platform teaming

AMSAA

/vid/phd/india/grss.99/vgs/g30

056

New Operational Challenges (cont)

- **Changing technologies:**
  - Rapidly expanding communications, sensor suites
  - New materials
  - Embedded processing

- **How do we use simulation and analysis* to focus on the right pieces (risk/design/capability/effectiveness) and understand how they fit together?**

* SMART (Simulation and Modeling for Acquisition, Requirements, and Training): Assistant Secretary of the Army (Acquisition, Logistics, and Training) approach to address OSD Simulation Based Acquisition.

AMSAA

/vld/phd/ndia/gvss.99/vgs/fg31

057

Extending the V/L Taxonomy

- The V/L Taxonomy

MOC

Risk Inputs → Platform Configuration → Platform Capabilities → Military Utility
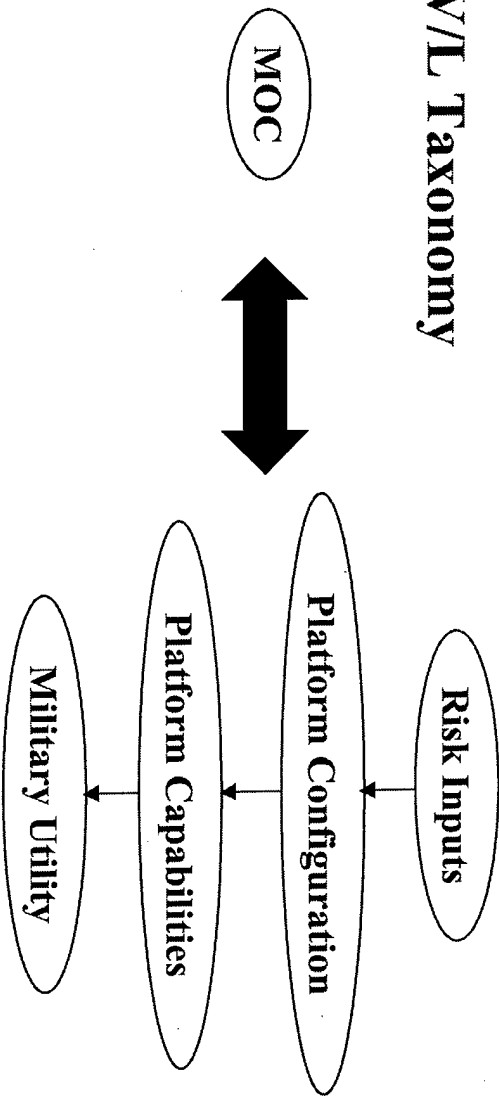
- With the following extensions:
  - Generalize the risk operator
  - Relate each level and operator to a Military Operational Context (MOC)
  - Use these connected metrics in a time-/event-stepped mission(s) script

058

Physical Analogues for the $O_{1,2}$ Operator

UNCLASSIFIED

AMSAA

/vid/phd/india/gyss.99/vgs/g50

Physical Analogues for the $O_{2,3}$ Operator

AMSAA

/vld/phd/ndia/gvss.99/vgs/g60
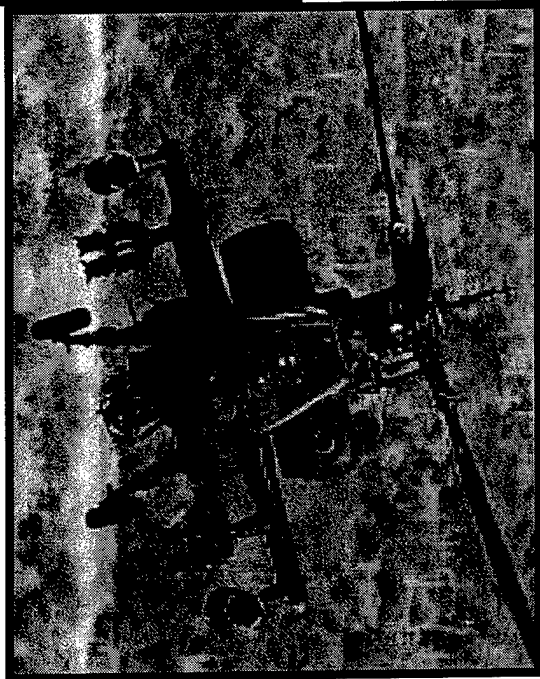
Physical Analogues for the $O_{3,4}$ Operator

AMSAA

/vid/phd/ndia/gvss.99/vgs/g70
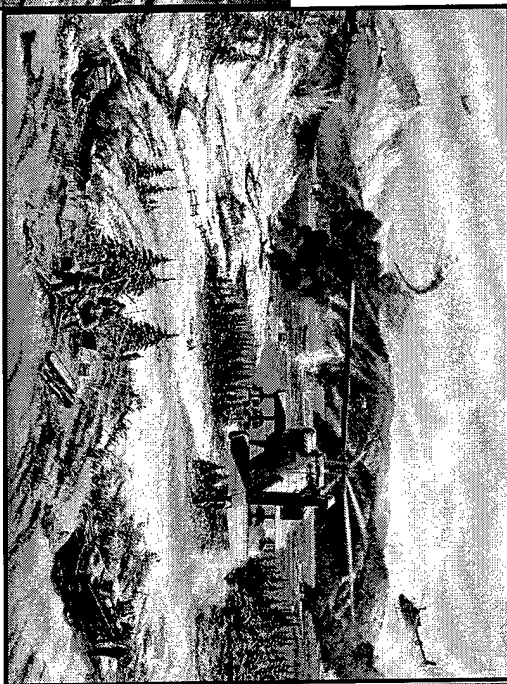
Generalizing the Live-Fire Operator

(Quasi-) Perm Damage	Temp Damage	Comp Repair/Fix
Ballistic	Electronic Jamming	Battle Damage Repair
Chemical	Cosite Interference	Resupply
Laser		
Directed Energy		
High-Pwr Laser		
Nuclear		
Physics of Failure		
Logistics Burdens (Fuel, Ammo)		
Reliability		
Fair Wear & Tear		

62

Mission-Based Acquisition Strategy

Level 1] - Initial
Conditions

Level 2] - Platform
Configuration Status

Level 3] - Platform
Capability Status

Level 4] - Mission
Outcomes Status

$O_{1,2}$ Change Operator

$O_{2,3}$ Capability Operator

$O_{3,4}$ Mission Operator

Risk Factors

Context Data

Msn Cap Reqs

Military
Operations
Context

•Tactics
•Doctrine
•Scenario
•etc.
(Global
Variables)

AMSAA

/vid/phd/ndia/gvss.99/vgs/g90

'63

Mission-Based Acquisition Strategy

Level 1] - Initial Conditions

9

8    $O_{1,2}$ Change Operator

Risk Factors

7

Military Operations Context

Context Data

•Tactics
•Doctrine
•Scenario
•etc.
(Global Variables)

Level 2] - Platform Configuration Status   4, 6

5    $O_{2,3}$ Capability Operator

Level 3] - Platform Capability Status   3

2    $O_{3,4}$ Mission Operator

Msn Cap Reqs

○ Subspace of vectors which map to a "success subspace" at the next Level

Level 4] - Mission Outcomes Status   1

Logic Instantiation/Exercise:

1 Define Desired Mission (s) Outcomes   4 Develop Point Designs   7 Develop Mission-Related Risk Factors

2 Develop Mission Mapping(s)   5 Develop Capability Mappings   8 Generate Required Change Operators

3 Define Mission-Relevant Capabilities   6 Estimate Cost for Each Design

9 Exercise logic to: a] assess risk(s), b] estimate any change in component status, c] estimate any change in platform capabilities, d] check mission outcome(s), if favorable, e] proceed to next mission task(s) or end of mission.

/kld/phd/ndia/gvss.99/vgs/g120

064

Summary

- **Have proposed a structure for SMART which:**
  - Shows connected platform and operational pieces
  - Shows the platform piece requires four distinct classes of metrics connected by three distinct classes of operators
  - Shows specific connections between the operational context and various platform metrics and operators

- **This illustrates a widespread class of Military OR problems. They are typified by the following:**
  1. Define baseline system configuration
  2. Estimate system performance
  3. Estimate system effectiveness
  4. Account for change in system configuration due to risks, *etc.*
  5. Go to 2., *etc.*

- **In SMART, the whole is greater than the sum of its parts. An adequate SMART analysis requires *all* pieces properly constructed, linked, and integrated.**

065

Summary (Cont)

- The *corner stone* of SMART should be the process of relating platform capabilities to desired mission outcomes (and *vice versa*) in the context of a highly resolved operational contexts. The $O_{3,4}$ Mission Operator and Level 4] Utility Status reflect our ability to understand what should become both the beginning and end of our analysis cycles, *operational success.*

- This process says that mission outcomes (including success) are related to platform capabilities, *not directly to technology.* Thus platform capability tradeoffs should be established in the context of mission performance first, then technology perused and exploited for opportunities to meet those capabilities (*i.e.*, requirements), subject to appropriate constraints. Thus:
  - Insight into manner in which the Operational, Technical, and Intel communities need to work together.
  - Implications for building the Army technology program.

AMSAA

^vid/phd/ndia/gvss.99/vgs/g140

066

Level 4] - Mission Outcomes Status
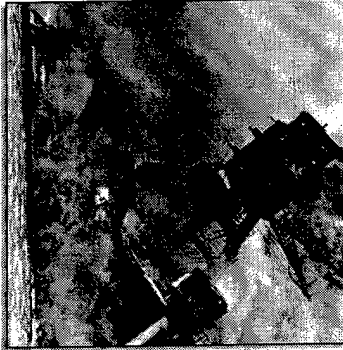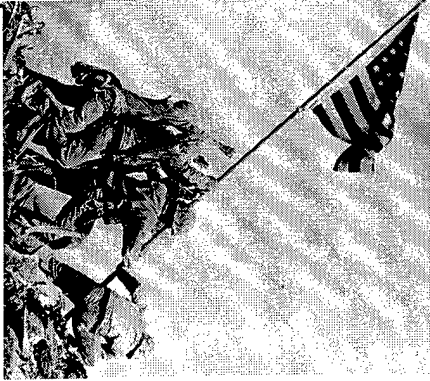
More US Marines won the Medal of Honor on Iwo Jima than in any other battle in US History. In 36 days of fighting there were 25,851 US casualties (1 in 3 were killed or wounded). Virtually all 22,000 Japanese perished.

Ahhaze, the Arizona sinks beneath the water
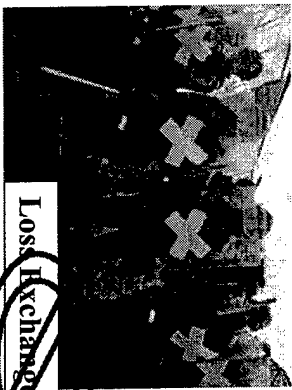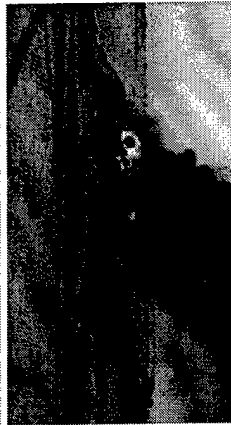
Loss Exchange Ratio (LER)
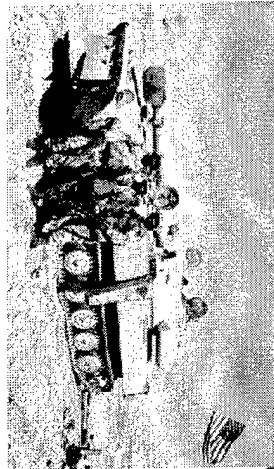
Measure? Avoidance

AMSAA

/vid/phd/ndia/gvss.99/vgss/g110

Conclusions

- Framework can be used to parse various M&S models to see where they fit into at least a significant portion of SMART. Can point to model duplication in some areas and lack of coverage in others.

- Framework can be used to set interface and architectural standards (per various Levels), make clear how algorithms are employed, highlight code gaps, and provide critical global connectivity.

- This decomposition shows that a large number of destructive (*e.g.*, ballistic, chem, nuclear, logistics burden, reliability) and constructive (*e.g.*, battle damage/expedient repair, product improvement process) operators require similar inputs, perform similar tasks, and modulate *identical* component status metrics.

- Illustrates that damage and repair/upgrade occur at Level 2]. Multiple instances of damage/repair must aggregate at Level 2], not, as is often done, by manipulating Level 4] metrics.

AMSAA

/vld/phd/ndia/gvss.99/vgs/g150

Conclusions (Cont)

- This approach can be used to analyze "Systems-of-Systems", *e.g.,* multiple communications platforms.

- Engineering issues focus on the $O_{2,3}$ operator. This operator takes Level 2] metrics and operational context data and must compute all capability metrics relevant, ultimately, to mission success. These include weights, moments-of-inertia, movement, all sensors, communications, guns/ missiles capabilities, *etc.* A large number of required engineering operators require similar inputs, perform similar tasks, and modulate *identical* capability status metrics.

- This process illustrates importance of global variables sourced in the MOC and coupled to various levels and operators.

^/id/phd/ndia/gvss.99/vgs/g160

069

Conclusions (Cont)

- Given a proscribed MOC (threats, mission, *etc.*), an inverse information threading can be established which points through critical performance factors, to supporting critical components and, finally, to any factors which put them at risk. These relationships can be used to prioritize which information and what strategies of test/model/analyze should be pursued.

- Costs and Benefits can be assigned with clarity to specific metrics and operators to support CAIV and AoA studies.

AMSAA

^/id/phd/ndia/gvss.99/vgs/g170

070

OPTIMIZING PLATFORM SURVIVABILITY USING A CHANCE CONSTRAINED LINEAR PROGRAM (U)

Jeffrey A. Smith
US Army Research Laboratory
Survivability\Lethality Analysis Directorate
Munitions and Platform Branch
White Sands Missile Range, NM 88002-5513

ABSTRACT (U)

(U) On today's battlefield, modern weapons are increasingly able to overmatch the protective capabilities of the armor on today's combat vehicles. The next generation of combat vehicles that the Army procures will need a combination of design strategies yielding a platform well suited to surviving on an increasingly lethal battlefield. Selecting the best design strategies, ones that yield a highly survivable platform, is a problem that the Army needs solved. The goal of this presentation is to demonstrate that optimum design approaches can be obtained as the solutions of a stochastic programming problem.

(U) Discussed is the problem of selecting a "best" set of design options or survivability measures when the performance of these options, as a function to the threat, is known, although the nature of the threat itself is stochastic. A solution to the selection problem is proposed under the assumption that the candidate suites work perfectly. The proposed approach is based on chance-constrained programming.

(U) The chance-constrained programming approach is attractive because it is intuitive and lends itself to a good engineering understanding of the process. Problems with a chance-constrained approach are discussed as well as areas needing additional research.

(U) INTRODUCTION

(U) Background

(U) One of the problems in designing the next generation of weapons platforms is that weapons designers are increasingly able to design weapons whose lethality exceeds the ability of armor to protect the platform. Platform designers can mitigate the effects of weapon lethality by incorporating design changes or active survivability measures of platform protection in addition to advanced armor. These mitigating approaches to platform survivability are called survivability measures.

(U) Survivability measures can include passive design strategies such as "stealthy" platform designs and other methods of lowering platform signature on the battlefield. These measures can also include active methods that search for and detect incoming threats, processing elements to determine the type of threat faced, and some threat defeat mechanism or countermeasure. There are many different concepts to choose from when deciding a suite of survivability measures, and each of these concepts have varying performance levels against each element of the threat array. In this context, concepts include notional systems, survivability components in development, and those survivability measures that have already been fielded.

(U) Choosing a "best" suite of survivability measures from among these various concepts in order to maximize platform survivability when the threat array is known is not difficult, and there are a number of approaches to deciding this "best" suite of survivability measures. However, the threat array is generally unknown or based on projections and expert assessment, which injects randomness into the threat array. The problem becomes much more difficult due to the variability inherent in the threat assessment. The platform designer will never know the exact nature of the threat array that a platform will face on a battlefield due to several factors. Among these factors are the lead time in designing and fielding the platform which implies that the threat array in existence at platform fielding will be estimated or projected based on expert assessment. Other factors include the

enemy who will engage the platform, the forces at their command, and even the location of the engagement. All these factors make the platform designer's job difficult.

<u>(U) Problem</u>

(U) When considering a platform's survivability, the current approach is to consider the four areas described in Figure 1. Each "avoidance" is approached differently. For example, a jammer is an active "hit avoidance" survivability measure, which may be used to defeat anti-tank guided missiles. Passive measures such as "penetration avoidance" may be approached by the addition of new or additional armor, and "detection avoidance" is approached through the use of designs minimizing, or masking, platform signatures. These avoidances are employed sequentially, i.e., if "detection avoidance" defeats a threat, then none of the other avoidances are needed. However, in practical situations a combination of survivability measures, addressing each of these avoidances will be needed to achieve the best possible platform survivability against each element of the threat array. For each of these avoidances, there are many survivability options, each with associated burdens (cost, weight, power and volume being common burdens) that are generally not functions of the threat array, and performance levels that are functions of the threat array. The problem then becomes selecting from among these many options the best possible set of survivability measures to maximize platform survivability against the overall threat array while minimizing burden to the platform.
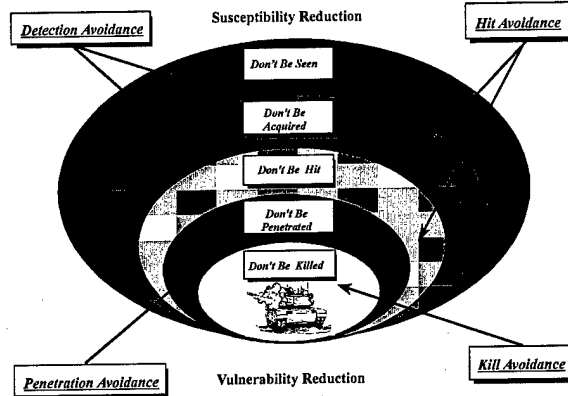
Figure 1: (U) Layered Survivability

<u>(U) PROBLEM STATEMENT</u>

(U) When I began to look at this problem, I made the following observations:

1. The list of survivability measures is discrete, and in a sense complimentary. A designer would likely choose a sensor and a defeat mechanism rather than two sensors or two defeat mechanisms by themselves.

2. This problem can be formulated in stages. If a platform is able to defeat a threat by avoiding detection, then the designer need not consider additional survivability measures for that threat. The same thought applies as you move inward on Figure 1; i.e., once a weapon is defeated no further protection is required. Ideally, the designer would like to defeat a threat as far out on Figure 1 as possible, and

3. The choice of one survivability measure may (or may not) impact the performance of follow on survivability measures, thereby affecting the choice of others; for example, a detection avoidance mechanism may also aid in acquisition avoidance.

(U) The last thing needed is a description of the notation used, and definitions of various probability measures that will be important for this discussion, and that is given in Table I.

Table I. (U) Notation

Variable	Meaning
W	The set of all warning sensors (each element is a single sensor)
C	The set of all countermeasures (each element a single countermeasure)
P	The set of all passive responses (each element is one design option)
P^X	The power set of a set X
A	The set of all active suites and is $\{(w, c) \mid w \in P^W, c \in P^C\}$
S	The set of all survivability suites and is $\{(p, a) \mid p \in P^P, a \in A\}$
Ω	The set of all threats

(U) Two probability measures are used when discussing platform survivability. These measures are the probability of kill and the probability of survival; both these measures are related to Figure 1. The probability of kill is given by:

$$P_k(s, \omega) = \Pi \ P_i(s, \omega) \text{ for } i = 1,2,3,4$$

where

$s \in S$,

$\omega \in \Omega$,.

$P_1(s, \omega)$ = the probability the threat detects the platform,

$P_2(s, \omega)$ = the probability the threat acquires the platform, given that the platform was detected,

$P_3(s, \omega)$ = the probability the threat hits the platform, given platform acquisition, and

$P_4(s, \omega)$ = the probability the threat kills the platform, given a platform hit.

(U) The probability of survival is one of the most important measures of performance a platform designer keys on in the design. The probability of survival for a given platform is given by:

$$P_s(s, \omega) = 1 - P_k(s, \omega).$$

Note: as formulated $P_i(s, \omega)$ may have different values depending on the successful operation of the active survivability measure in s (the a portion of s).

APPROACH

(U) Chance-constrained models relax the feasibility requirement imposed upon a traditional linear program. In a linear program a feasible solution is one that meets all of the constraints. A chance-constrained program allows some, or all of the constraints to be met at a specified level of confidence. Chance-constrained models were first introduced by Charnes and Cooper [ref. 4] and expanded by Van De Panne and Popp [ref. 24], Miller and Wagner [ref. 16] as well as others. Other excellent references include the classic texts by Vajda [ref. 23] and Kall [ref. 13]. Chance-constrained models arise when exact values of some of the problem parameters are not known, such as the nutritive content of cattle feed problem discussed by Van De Panne and Popp.

(U) The selection problem formulated as a chance constrained program is:

$$\min c^T s,$$

$$\text{subject to } A_{dc}s \leq b_{dc}, \text{ and}$$

$$P(\, P_k(s, \omega) \leq \beta \,) \geq \alpha \,) \, (0 < \alpha < 1, 0 < \beta < 1),$$

where c is a cost vector, A_{dc} is a matrix of purely deterministic design criterion, b_{dc} is a vector of deterministic design goals, $s \in S$, $\omega \in \Omega$, and the final constraint is the chance constraint. For the selection problem at hand, this constraint represents the probability that the threat succeeds in killing the target, $P_k(s, \omega)$, is less than some desired level β, and this constraint is met with a probability α. An equivalent representation of the chance constraint base on survivability yields the following:

$$P(\, P_s(s, \omega) \geq 1 - \beta \,) \geq \alpha \,).$$

where α and β are defined as above.

(U) Miller and Wagner indicated that if the following condition was true, a log transform of the product in the chance constraint allows replacement of the probability product with a sum of the log probabilities [ref. 16].

$$-d \ln P_s(s, \omega) \,/\, d\omega = p_k(s, \omega) \,/\, [\, 1 - P_k(s, \omega) \,] \equiv q(s, \omega), \text{ for } P_k(s, \omega) < 1,$$

where $q(s, \omega)$ is called the hazard rate, s and ω are defined as above. If $q(s, \omega)$ is an increasing function, then $\ln P_s(s, \omega)$ is concave, and therefore the product constraint is defined on a convex set. Taking the log of the chance constraint allows us to place the selection problem in a form that is solvable by linear programming methods. This yields:

$$F(s, \omega) = - \ln \beta + \Sigma \ln P_i(s, \omega) \text{ for } i = 1, 2, 3, 4.$$

(U) In addition to Miller and Wager, several others have presented related work regarding log-concavity and convex measures. Van De Panne and Popp [ref. 24] established the conditions under which the chance constraint is a convex constraint for joint normal distributions. Prekopa's work in [ref. 19] is widely regarded as an important generalization of log concave measures in stochastic programming. Prekopa established the general conditions under which the feasible set for a chance constraint is a convex set. Vajda notes that, while many commonly used distributions are not convex (e.g., normal and uniform), convex programming techniques can be used if by taking the log we obtain a sum of concave functions [ref. 23]. Finner and Roters [ref. 11] have studied log-concavity for the Chi-square, F and Beta distributions.

(U) Solution Methods

(U) Solution methods for chance constrained linear programs fall are either exact or approximate. Little has been written about exact solutions given the need to know the underlying distributions, but much has been written

on approximate solutions to chance constrained linear programs. Each of these approaches will be discussed in this section.

(U) When the distributions and parameters characterizing them (means and covariances) are known, solving chance-constrained programs is done by replacing probabilistic constraint with a deterministic equivalent based on these parameters. Vajda [ref. 23], Kall [ref. 13], Mitra [ref. 17], and Sposito [ref. 21] are good references for this depending on the nature of the problem. Szantai [ref. 22] presents a computer code for solving these problems when the resulting distributions are normal. Prekopa discusses several approaches to solving chance-constrained models in [ref. 20] including gradient methods and the use of penalty functions. Eisner and Olson discuss the use of duality in solving chance constrained models [ref. 8].

(U) While there are methods of solving chance-constrained programs exactly, there are many practical cases in which it is not possible to solve the system in an exact form. Many people have suggested approximate solutions, which can be grouped into three categories. The first and most extensive category is that based on interval or bounding techniques. The second category involves replacing the chance constraint by a linear approximation, and the final category is a relaxation technique. Kall, Ruszczynski and Frauendorfer survey of various approximation approaches in [ref. 15], discussing worst case analysis, discrete approximations, bounding, and other techniques.

(U) Among the interval or bounding techniques, Hillier [ref. 12] presents both an exact and an approximate solution when the decision variables are zero/one constrained or continuous. Hillier's technique involves placing upper and lower bounds on the chance constraint, where these bounds are estimated or calculated from the parameters of the distributions. Hillier's method seems well suited for use when the number of points needed to estimate the bounds is small. Allen, Braswell and Rao [ref. 2] discuss a method that does not depend on the distribution, but on a tolerance region and sample. These authors also show how the chance constraint set can be transformed into a distribution free set of constraints. Dupacová discusses an approach based on worst case, or expert assessment of the resulting distribution, and then he uses these to approximate the chance constraints [ref. 7].

(U) Linear approximations of the chance constraints are the second major category of approximation approaches. In all, I've selected four papers as representatives of this approach. In [ref. 5] Charnes, Kirby and Raike introduce the concept of an acceptance region. They use the concept of an acceptance region to establish the presence or absence of an optimal solution. When an optimal solution exists, they show that there is an optimal piecewise linear decision rule that will find it. Olson and Swenseth present an approach based on a penalty function [ref. 18]. The authors use a linear approximation to the chance constraint, and then impose the penalty function, which as at least as great as the chance constraint. The advantage to this approach is that it is readily adaptable to joint distributions which are not independent. Olson and Swenseth also present the results of this linearization as they applied it to the problem Van De Panne and Popp solved in [ref. 24] with very good agreement. Akinfiev and Zharov present an approximation approach based on deterministic equivalents and apply that approach to a planning problem [ref. 1]. The final paper by Elsayed and Ettouney [ref. 9] replaces the chance constraint with one based on a Taylor series expansion and then solves the resulting program recursively to a desired tolerance level. Elsayed and Ettouney also apply the Taylor series expansion to two examples and present the resulting solutions.

(U) The final approximate solution category contains a paper by Charnes, Chang and Semple [ref. 3]. In this paper, the authors discuss the concept of relaxation applied to the chance constraint. They propose a method of relaxing a set of joint constraints into a semi-infinite set of individual constraints. The paper also develops tight relaxation to constraints where only partial distribution (mean and variance) information is known. The authors also apply this technique to examples provided by Prekopa and Szantai with good agreement.

(U) Within the three categories of approximations above, five papers present approaches that should be applicable to solving the selection problem. The papers are those by Hillier [ref. 12], Charnes, Kirby and Raike [ref. 5], Olson and Swenseth [ref. 18], Elsayed and Ettouney [ref. 9], and by Charnes, Chang and Semple [ref. 3]. All of the papers present approaches that appear, with little modification, to be readily adaptable to problems with dependence or conditional distributions in addition to being readily useable for problems with independent joint distributions.

(U) SUMMARY

    (U) Weapons designers are increasingly able to field weapons whose lethality easily overmatches the armor on both current and next generation weapons platforms. Platform designers can mitigate the effects of weapon lethality by incorporating design changes or active survivability measures of platform protection in addition to advanced armor. These mitigating approaches to platform survivability are called survivability measures, and the set of measures applied to a platform is called a survivability suite.

    (U) The recognition that a designer may not be able to achieve 100 percent survivability against all threats suggests a situation where relaxing the survivability criteria allows one to achieve a "optimum" solution. This is chance programming. The possibility of inter-relationships among some combinations of survivability measures in a suite (either a mutual degradation or a synergy where the whole is greater than the sum of the parts) suggests approaches that allow interactions to occur. That is the incorporation of a covariance matrix into the analysis process.

    (U) When the designer makes the assumption a selected survivability suite works probabilistically, and that 100% survivability is unattainable, the selection problem lends itself to a chance programming approach. The chance programming approach, from an engineering perspective, is intuitive. The deterministic constraints are ones that the designer can know or estimate very well, and the design goals are ones that are easily understood. The objective function, in this sense, is not important if the designer leaves the coefficients set to unity. However, by changing the weights of the objective function, the designer can create preferences for certain solutions. For example, notional designs, which may not be the preferred course of action, may have a "cost" higher than survivability designs already completed. Only if the notional design is considerably better than what is already completed will the notional design be chosen. Again, this is an intuitive feature. And finally, the chance constraint is easily understood from a systems engineering viewpoint.

    (U) Several problems should be noted. The first problem is actually the assumption that the survivability suite works properly. In a real world situation this is not the case, but the assumption is a good one for establishing an upper bound on anticipated performance levels. Furthermore, this assumption allows a very good first cut at solving the selection problem.

    (U) The second problem relates to the first problem in the sense that to truly optimize survivability, the performance of the suite should be modeled as well. For example, there is a small, but non-zero probability that a threat classifier may miss-identify a threat. A survivability suite that is a robust performer against a wide array of threats should account for the functioning of the survivability components as well.

    (U) The final problem is that this while approach may lend itself to selecting a "best suite," it may miss solutions where a combination of "active" (active sensor/countermeasure combination) and "passive" approaches may yield better survivability (additional armor and signature minimizing designs). Coupling both approaches may yield better survivability against a broader class of threats, but the chance programming approach seems to lend itself to one or the other type of approach, but generally not both.

(U) CONCLUSION

    (U) Selecting the components of a survivability suite is a problem in stochastic programming and it has the potential for research in a number of different areas. The three problems identified in the summary all present a degree of difficulty and all of them will require a good deal of study to solve. The selection problem, cast as a chance constrained program, is a good first step in defining a method for selecting a best set of survivability options.

    (U) The Army survivability community needs a tool that can optimize a platform's survivability against a broad array of threats. A method that can determine a "best" suite of survivability measures is something that can benefit the Army's survivability community as a whole. The selection of this "best" set of survivability measures is a stochastic programming problem, and the first step in creating the methodology is by exploring chance programming.

UNCLASSIFIED

(U) REFERENCES

1. V. K. Akinfiev and T. M. Zharov "Programming The Expansion Of Large-Scale Systems Allowing For Uncertainty And Risk Factors," Avtomatika i Telemekhanika, 52, no.8, 155-66 (August 1991), Automation and Remote Control, 52, no.8, pt.2, 1160-7 (August 1991).

2. F. M. Allen, R. N. Braswell and P. V. Rao "Distribution-Free Approximations For Chance Constraints," Operations Res. 22, 610-621, (1974).

3. Charnes, Y. C. Chang and J. Semple "Semi-Infinite Relaxation of Joint Chance Constraints in Chance-Constrained Programming. Part 1. Zero-Order Stochastic Decision Rules," International Journal of Systems Science, vol.23, no.7, 1051-61 (July 1992).

4. Charnes and W. W. Cooper "Chance Constrained Programming," Management Science, 6, 73-79, (1959).

5. Charnes, M. J. L. Kirby and W. M. Raike "An Acceptance Region Theory For Chance-Constrained Programming," J. Math. Anal. Appl. 32, 38-61, (1970).

6. M. A. H. Dempster (ed.) Stochastic Programming, Proceedings of an International Conference Sponsored by the Institute of Mathematics and Applications, Mathematical Institute, Oxford, 15-17 July 1974, Academic Press, New York, 1980.

7. J. Dupacová "On Interval Estimates for Optimal Value of Stochastic Programs," " in [ref.14], 556-563.

8. Mark J. Eisner and Paul Olsen "Duality In Probabilistic Programming," in [ref.6], 147-158.

9. E. A. Elsayed and Mohammed Ettouney "Perturbation Analysis Of Linear Programming Problems With Random Parameters," Comput. Oper. Res. 21, No.2, 211-224, (1994).

10. Yu. Ermoliev and Roger J-B Wets (Eds.) Numerical Techniques for Stochastic Optimization, Springer Series in Computational Mathematics; 10. Springer-Verlag, New York 1988.

11. H. Finner and M. Roters "Log-Concavity and Inequalities for Chi-Square, F-Distribution and Beta-Distribution with Applications in Multiple Comparisons," Statistica Sinica, 7, no. 3, 771-787, (July 1997).

12. Fredrick S. Hillier "Chance-Constrained Programming with 0-1 or Bounded Continuous Decision Variables," Management Science, 14, no. 1, 34-57, (1967).

13. Peter Kall, Stochastic Linear Programming. Econometrics And Operations Research (Okonometrie Und Unternehmensforschung), 21, Springer-Verlag, New York, 1976.

14. Peter Kall (Ed.), System Modeling and Optimization, Proceedings of the 15th IFIP Conference, Zurich, Switzerland, September 2-6, 1991. Springer-Verlag, New York, Lect. Notes Control Inf. Sci. 180, 1992.

15. Kall, A. Ruszczynski and K. Frauendorfer "Approximations in Stochastic Programming," in [ref.10], 33-64.

16. Bruce L. Miller and Harvey M. Wagner "Chance Constrained Programming with Joint Constraints," Operations Research 13, 930-945, (1965).

17. Gautam Mitra, Theory and Application of Mathematical Programming. Academic Press, New York, 1976.

18. D. L. Olson and S. R. Swenseth "A Linear Approximation For Chance-Constrained Programming," Journal Of The Operational Research Society, 38, No.3, 261-267, (March 1987).

19. Prekopa "Logarithmic Concave Measures and Related Topics," in [ref.6], 63-82.

UNCLASSIFIED

20. Prekopa "Numerical Solution of Probabilistic Constrained Programming Problems," in [ref.10], 123-140.

21. Vincent A. Sposito, Linear Programming With Statistical Applications. Iowa State University Press, Ames, 1989.

22. T. Szantai "A Computer Code for Solution of Probabilistic-constrained Stochastic Programming Problems," in [ref.10], 229-236.

23. S. Vajda, Probabilistic Programming. Probability and Mathematical Statistics Series 9, Academic Press, New York, 1972.

24. Van De Panne and W. Popp "Minimum-Cost Cattle Feed under Probabilistic Protein Constraints," Management Science, 9, 405-430, 1963.

CHEMICAL DETECTION ON MOBILE AND ARMORED VEHICLES (U)

Daniel M. Nowak

U.S. Army Soldier and Biological Chemical Command
Project Manager for Nuclear, Biological, and Chemical Defense Systems
Aberdeen Proving Ground, MD 21010-5424

ABSTRACT (U)

(U)   The use of chemical warfare (CW) agents continues to be a viable
threat to U.S. Forces around the world. Given the increasing peacekeeping
nature of the U.S. Forces, effective countermeasures to CW agents are
necessary. Within the last few months the U.S. Army has taken delivery of a
new chemical agent detector, the M22 Automatic Chemical Agent Alarm
(ACADA). This is a major advance in the equipping of the U.S. Army's
mounted force to face this continuing threat.

(U)   The ACADA is the most advanced chemical warfare detector to be
fielded by the U.S. Armed Forces. The ACADA detects the most common
nerve and blister agents and can be programmed to address other agents. The
system is designed to be point detector installed in vehicles, used by the
infantry and deployed around fixed sites as a perimeter defense system.

(U)   The ACADA is a rugged and self-contained unit, which can provide
early warning of gas attack. This warning can be given by a local or a remote
audio/visual alarm. The ACADA system has been developed complete with
vehicle mount. This can provide protection for the detector in the harshest
vehicle environment and facilitate the use of the vehicle electrical supply to
power the unit. The system is scheduled to be installed on the FOX, M1A2
Bradley, HMMWV and the M113.

(U)   Within the presentation, the ACADA Program Team will briefly
review the ACADA test program, detail the performance of the unit, give
details of the current vehicle programs and describe the support and training
available from the program office.

(U)   The ACADA was developed by a commercial company, Graseby
Dynamics Limited, working closely with the U.S. Army Soldier and Biological
Chemical Command (SBCCOM) at Aberdeen Proving Ground, Maryland.

(U)   The use of Chemical Warfare agents continues to be a viable threat to U.S. Forces. In an interview for the United States Navy Surface Warfare Magazine, Major General Wooten, Commandant of the U.S. Army Chemical School stated "The chemical/biological threat is real, more so than the nuclear threat right now. Before the demise of the Soviet Union, we believed the chemical/biological threat was contained. But when "the wall" crumbled, there was no more central control; chemical/biological weapons and weapon delivery systems proliferated. Intelligence estimates 25-27 countries have either chemical or biological weapons." (ref. 1) Chemical Agents have been called "poor man's nuclear weapon". The manufacture of chemical warfare agents in small quantities by terrorists is an ongoing threat but the manufacture and use of military quantities of chemical warfare agents for delivery against U.S. Forces during military missions is always a potential. The delivery of chemical weapons against our ground and mechanized forces could cause disruption of communications and a degradation of command and control. There are numerous defense strategies for countering these threats and the newest tool in ameliorating the tactical effects of chemical agents is the M22 Automatic Chemical Agent Alarm, ACADA (Slide 1). The M22 ACADA is the Joint Services most advanced chemical agent detector. It is a point detector which is capable of quickly warning our troops that a chemical attack has occurred or that our forces have traversed a chemically contaminated area. Chemical agents are colorless and in many cases odorless chemicals, which at very low concentration, can cause incapacitation and lethal effects on personnel (Slide 2). With sufficient warning, military personnel can take protective measures to reduce the chances of inhaling these chemical warfare agents, thereby preventing or reducing casualties (Slide 3). The M22 ACADA, when employed properly, will provide this warning capability. The M22 simultaneously senses vapors of Nerve and Blister agents and provides an alarm. It is programmable for other threat agents. The detector is highly resistive to interferences. The M22 system consists of the M88 detector, transit case, removable battery pack and M42 remote alarm unit. Auxiliary equipment includes the M28 power supply and M281 vehicle mount with an M42 mounting bracket (Slide 4).

(U)   M22 is designed for 3 operational roles. These roles include area warning, monitoring collective protective equipment (CPE) and operation on and in vehicles. In the area warning role, the M22 is employed up to 400 meters upwind and is operated by a battery pack (Slide 5). The hard wired M42 alarm unit is emplaced with the troops to be alerted. Once operational, set-up and break-down times are typically a few minutes, making the system highly mobile for changing tactical situations. In the CPE monitoring role (Slide 6) the M88 detector is used with the M28 power supply to allow long term monitoring of the air. This operational role will indicate if the "clean" environment has been breached by incoming contaminated personnel or equipment, or if the chemical filters have failed.

(U)   In the vehicular role (Slide 7) the M88 detector is used with the M281 vehicle mount and powered from vehicle power. In this application the M88 detector can be installed at an appropriate location on the exterior or interior of the vehicle. Both applications require the M281 vehicle mount which provides vibration and shock isolation for the detector. The M42 is connected to the M88 alarm and located near crew members to provide an audible and visual alarm. The M88 is the detector used with the Multi-Purpose Integrated Chemical Agent Alarm (MICAD) system. The MICAD system is used for communication to the immediate crew and surrounding command and control units that a chemical agent has been detected in or around a particular vehicle. The M88 detector is easily removed from the M281 vehicle mount to allow for area warning around the vehicle.

(U)   The M22 system is the most extensively tested chemical detector fielded to U.S. Forces (Slide 8). The 2 year test program included all military environmental and intended operational roles. Test conditions included operation at temperature extremes of –30 degrees Centigrade to +55 degrees Centigrade, rain, dust, salt spray and electro-magnetic interference including high altitude electro-magnetic pulse. Extensive vehicular tests (Slide 9) were conducted at the Test and Evaluation Command test sites in Alaska, Panama, Yuma, and Aberdeen. The detectors were mounted on the exterior of the vehicles to demonstrate reliability and survivability. In the Arctic, the Small Unit Support Vehicle (SUSV) and High Mobility Multi-Purpose Wheeled Vehicle (HMMWV) were tested at temperatures down to
-45 degrees Centigrade and were driven a total of 200 vehicular miles. At the Tropic Test Center, the M22 was mounted on the HMMWV and operated in driving rain and in tropic conditions for a total of 1,182 vehicular miles. At the Desert Test Center, the M22 was mounted on the M113 Armored Personnel Carrier (APC) and operated in dusty conditions and at temperatures up to 50 degrees Centigrade. At this location, a total of 2,760 vehicular miles were accumulated. At the Aberdeen Test Center (ATC), testing consisted of the M22 being mounted on the outside of the M113 APC and at the center console of the HMMWV. Both vehicles accumulated a total of 10,000 vehicular miles while being driven over the Perryman Cross-Country vehicle qualification courses. In all cases, the M22 and its vehicle mount operated successfully and without false alarm. An additional test was conducted (Slide 10) at ATC to qualify the M22 for attack vehicles. The M22 was mounted both inside and outside the M1A1 Main Abrams Battle Tank using the vehicle mount. The M1A1 cannon was fired to determine if the blast, shock and combustion effluents would effect the operation of the M22. The M22 operated successfully throughout the test.

(U)   The M22 is rugged, not prone to interferences and is very sensitive to chemical agents. Its application on vehicles is the next step for providing our mechanized forces with the warning and information essential to protect the crew and to avoid contamination of their equipment. Currently, the M22 (Slide 11) is being installed in all M93A1 Nuclear Biological Chemical Reconnaissance Systems (FOX vehicles) and the M22 is a requirement on the Bradley Command Control Vehicle (C2V), the Advanced Amphibious Assault Vehicle (AAAV) and Light NBC Recon. The M22 can be applied to many types of platforms including the M113, HMMWV, Crusader, Paladin, Future Scout Vehicle, SUSV, M2 Bradley, and M1 Abrams. Applications on other vehicles are also viable.

(U)   Graseby, the developer of the GID 3 (Slide 12) (which was designated the M22 by U.S. Forces) has fielded the detector on vehicles from several countries including Canada, United Kingdom, and Kuwait. The use of vehicles as mobile platforms for detecting a chemical threat will require development of doctrine but has the potential to provide warning to a mechanized company independent of ground troops. At a minimum, the M22 detector mounted on the vehicles, will provide the crew with a level of warning to protect both themselves and their equipment or to engage collective protective equipment, if available.

(U)   The ACADA team is dedicated to product support and we have several (Slide 13) publications available or in development to assist operators and users in the deployment and operation of the M22. These include technical manuals, bulletins, a CD ROM, and an operator's video.

(U)   For more information (Slide 14) on the ACADA program, contact either myself or Mary Beth Morris. For technical assistance, contact Graseby representatives Mr. Bloomfield or Mr. Langford.

Reference:

1. Surface Warfare Magazine, November/December 1996, "The Battle of NBC", p. 16 (U).

TARGET CLASSIFICATION VIA SUPPORT VECTOR MACHINES

Robert E. Karlsen, David J. Gorsich and Grant R. Gerhart

U.S. Army Tank Automotive Research, Development and Engineering Center
Warren, MI 48397-5000

ABSTRACT

The area of automatic target classification has been a difficult problem for many years. Many approaches involve extracting information from the imagery through a variety of statistical filtering and sampling techniques, resulting in a reduced dimension feature vector, which can then be input to a learning algorithm. In this paper, we outline a method that is virtually independent of feature vector size and can therefore be applied to entire images, so that the feature extraction and learning algorithm are combined into one. We present the results of two image classification tests, both of which yielded excellent results.

Introduction

The problem that we address in this paper is image classification. Specifically, we consider algorithms that can take as input a digital image and classify it according to some criterion. Often this is a three-step process, consisting of pre-processing, feature extraction, and decision algorithm. The pre-processing is used to remove redundant information or to transform the image to a space where the objects are more easily classified. We have used the multiresolution approach in previous applications, implemented through the fast wavelet transform[1-3]. The feature extraction step is employed to reduce the dimensionality of the problem. Examples of features include peaks in the Fourier spectrum, statistical measures of edge densities, multiresolution energies or a histogram of gray levels. The final step is the decision module, which takes as input the lower dimension feature vector and outputs the classification. Often the decision algorithm is also a learning algorithm. In this case, a sufficiently large number of sample images, with their associated classification, are presented to the algorithm. The algorithm then adjusts certain parameters in order to satisfy a minimum error criterion.

The typical learning algorithm is a neural network (fuzzy logic systems generally have an embedded neural network for automated learning). The reason that feature vector selection is so important for neural networks (specifically back-propagation neural networks) is that the complexity of the network scales with the size of feature vectors. In fact, the number of free parameters that must be determined is proportional to the size of the feature vector and is often many times larger. This generally necessitates a large number of training samples in order to constrain the error minimization sufficiently.

The Support Vector Machine (SVM) algorithm[4-6] avoids many of these problems. Here, only the dot product between feature vectors enters the problem. Therefore, the length of the feature vector has little effect on the computational complexity of the algorithm. By design, SVM is a large margin classifier, and can give reasonable results even for sparse training sets, where the number of samples may be less than the size of the feature vector. SVM can also be made resistant to outliers of a given size, by adjusting a cost parameter.

The paper begins by providing a brief tutorial on Support Vector Machines and outlining derivations of some of the important elements. We then use the SVM algorithm on two data sets, the first is a standard handwritten digit data set[7], derived from two NIST data sets, and the second is a collection of images of military vehicles. Both of these were classified accurately with SVM. We conclude by summarizing our results and indicating the future direction of our research.

Support Vector Machines

To introduce the Support Vector Machine (SVM), we first consider a linearly separable problem; i.e. the data can be separated completely by a hyperplane. Figure 1 shows an example in two dimensions, where the hyperplane is a line. The object is to find the best hyperplane that separates the data into two classes, where, by 'best' we mean the hyperplane that gives the best classification results when new data is used.
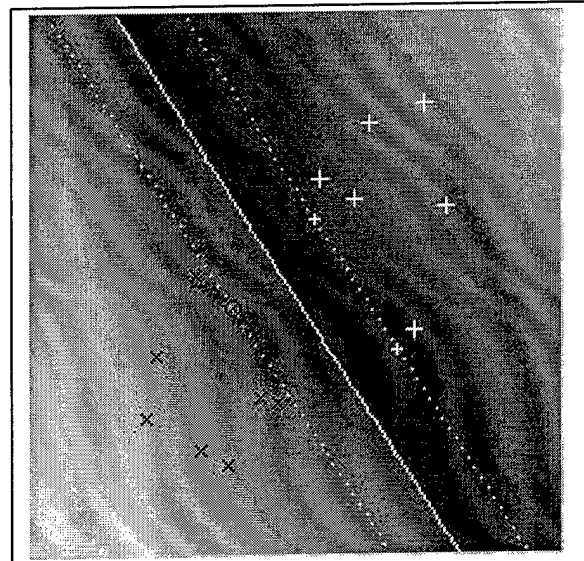
The SVM algorithm[4-6] is based on finding a pair of parallel hyperplanes, which separate the data and which have the largest perpendicular distance between them. It is conjectured that this will provide a good approximation to the 'best' separating hyperplane. Each data point is described by a feature vector $\bar{x}$ and a truth value y, the latter of which can take the values of +1 or −1, depending on the class. The two hyperplanes are required to pass through at least one point of each class and there can be no points between them. The boundary between the classes is then defined to be a third parallel hyperplane that is halfway between the other two. The data points that the outer hyperplanes pass through, which are circled in Fig. 1, are called the support vectors, the meaning of which will be explained later. The two outer hyperplanes are described by the following expressions,

Fig. 1: Linearly separable data.

$$\bar{w} \cdot \bar{x} + b = +1,$$
$$\bar{w} \cdot \bar{x} + b = -1, \tag{1}$$

with the first going through a point of class $y=+1$ and the second going through a point of class $y=-1$. The constants $\bar{w}$ and b define the hyperplanes, with $\bar{w}$ being normal to the hyperplanes and $-b/\|\bar{w}\|$ being the perpendicular distance from the origin to the middle hyperplane. The RHS of Eq. (1) will be greater than or equal to +1 for all points of class $y=+1$ and will be less than or equal to −1 for all points of class $y=-1$. These can be combined into the following constraint on all the data points,

$$y_i\left(\bar{w} \cdot \bar{x}_i + b\right) - 1 \geq 0. \tag{2}$$

The perpendicular distance between the two outer hyperplanes is equal to $2/\|\bar{w}\|$. Therefore, finding the hyperplanes with the largest margin reduces to finding values for $\bar{w}$ and b that minimize $\|\bar{w}\|^2$, subject to the constraint in Eq. (2).

A standard method for handling optimization problems with constraints is through the minimization of a Lagrangian[8-10]. The constraints are taken into account by adding terms involving Lagrange multipliers to the objective function. In this case, this results in the following primal Lagrangian[4-6],

$$L_P = \frac{1}{2}\|\bar{w}\|^2 - \sum_i \lambda_i y_i\left(\bar{w} \cdot \bar{x}_i + b\right) + \sum_i \lambda_i \tag{3}$$

where λ_i are the Lagrange multipliers associated with each of the constraints in (2). Notice that at the boundary of the constraint equation (2), the extra terms added in (3) are zero. As one moves away from the boundary, the Lagrangian becomes smaller. Because the constraints are inequalities, bounded from below, the Lagrange multipliers are required to be non-negative.

Setting the derivative of the Lagrangian in (3) with respect to $\vec{w}$ and b (the primal variables) equal to zero, results in the following expressions,

$$\vec{w} = \sum_i \alpha_i y_i \vec{x}_i, \tag{4a}$$

$$\sum_i \alpha_i y_i = 0, \tag{4b}$$

while from the definition of the Lagrange multipliers, we obtain,

$$\alpha_i\left(y_i\left(\vec{w}\cdot\vec{x}_i + b\right)-1\right)= 0. \tag{4c}$$

Inserting Eqs. (4a) and (4b) into (3), results in the dual Lagrangian,

$$L_D = \sum_i \alpha_i -\frac{1}{2}\sum_{i,j} \alpha_i\alpha_j y_i y_j \vec{x}_i\cdot\vec{x}_j. \tag{5}$$

The problem is now reduced to finding the Lagrange multipliers (the dual variables) that maximize Eq. (5) and satisfy both the non-negativity constraints and the constraints of Eq. (4b). Equation (4c) means that only those data points which lie on the outer hyperplanes (and hence are active constraints) will have non-zero Lagrange multipliers. These data points are called the support vectors and they are the points that determine the position of the hyperplanes. One can move the other points around the feature space or remove them entirely and the solution will not change, provided one does not move a point across one of the outer hyperplanes.

The relationships in Eqs. (4), together with the constraints in Eq. (2) and the non-negativity constraints on the Lagrange multipliers make up what are known as the Karush-Kuhn-Tucker[8-12] (KKT) conditions for this particular problem. The KKT conditions are general rules that arise in constrained optimization problems, and finding solutions that obey them generally results in an optimal solution. Since SVM is a quadratic-programming problem (the objective function, $\|\vec{w}\|^2$, is quadratic) with linear constraints, the KKT conditions are necessary and sufficient for the resulting $\vec{w}$, b and α to be an optimal solution. One can solve Eq. (5) using any quadratic programming solver, although different solvers perform better on different types of problems[6,8-10]. Solving the quadratic programming problem is actually one of the most difficult parts of SVM and will not be discussed further in this paper.

Fig. 2: Non-linearly separable data.

Once the Lagrange multipliers are known, the solution for $\vec{w}$ is given by Eq. (4a), where the sum is over the support vectors, since they are the only ones with non-zero α. One can find b from Eq. (4c), using any of the support vectors, although one generally averages over all the support vectors for better accuracy. Once these constants are known, the classification of an unknown vector, $\vec{v}$, is given by the sign of,

$$b+\sum_i \alpha_i y_i \vec{x}_i\cdot\vec{v}, \tag{6}$$

where the sum is over the support vectors. This determines on which side of the boundary (or middle) hyperplane that the data point falls.
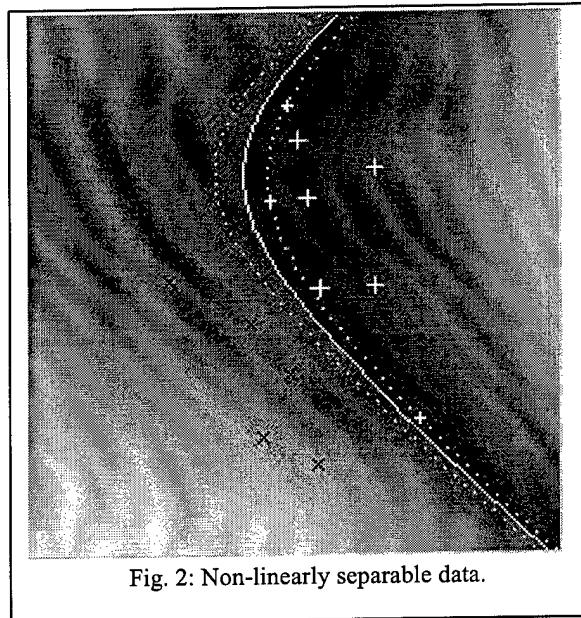
Now suppose that the boundary between the data is nonlinear. An example of this situation is shown in Fig. 2. One cannot separate the two classes with a straight line. The structure of the SVM equations allows a simple solution to this situation. Map the data, through a nonlinear transformation , to a different space, where the data can be separated with a hyperplane. This results in the Lagrangian in (5) being transformed to,

$$L_D = \sum_i {}_i - \frac{1}{2}\sum_{i\ j} {}_i {}_j y_i y_j \ (\bar{x}_i) \cdot \ (\bar{x}_j), \tag{7}$$

and the classification relation in Eq. (6) becomes,

$$b + \sum_i {}_i y_i \ (\bar{x}_i) \cdot \ (\bar{v}). \tag{8}$$

Since Eqs. (7) and (8) depend only on the dot product between the two transformed feature vectors, one can employ a kernel function,

$$K(\bar{x}, \bar{y}) = \ (\bar{x}) \cdot \ (\bar{y}), \tag{9}$$

and never need to computer the transformation explicitly. Equation (8) then becomes,

$$b + \sum_i {}_i y_i K(\bar{x}_i, \bar{v}), \tag{10}$$

with the test feature vector now inside the summation over the support vectors.

In general, the mapping will be to a higher dimensional space. For example, suppose the data is in two dimensions and the kernel is $K(\bar{x}, \bar{y}) = (\bar{x} \cdot \bar{y})^2$, then the mapping could be to three dimensions (but not to two) with either of the transformations (among others),

$$(\bar{x}) = \begin{pmatrix} x_1^2 \\ \sqrt{2}x_1 x_2 \\ x_2^2 \end{pmatrix} \quad \text{or} \quad (\bar{x}) = \frac{1}{\sqrt{2}} \begin{pmatrix} x_1^2 - x_2^2 \\ 2x_1 x_2 \\ x_1^2 + x_2^2 \end{pmatrix}, \tag{11}$$

or the mapping could be to four dimensions,

$$(\bar{x}) = \begin{pmatrix} x_1^2 \\ x_1 x_2 \\ x_1 x_2 \\ x_2^2 \end{pmatrix}, \tag{12}$$

where the subscripts in all cases refer to components of the vector $\bar{x}$. The kernel remains the same in each case and the resulting classification results are identical. Since one is still solving the linear problem, just in a different space, the computational overhead is essentially the same. The solution and parameters for the hyperplane are in the higher dimensional space and when one transforms back to the original space the boundary becomes nonlinear. However, there is, in general, no way to analytically invert the solutions for $\bar{w}$ and b. Hence, one must use Eq. (10) to classify test feature vectors.

The advantage to using the kernel approach is that the higher dimensional (or embedding) space is essentially hidden from the user. One, in fact, never needs to know the function . It could even be of infinite dimension. The disadvantage is that one must use Eq. (10) to classify each test vector and if there are a large number of support vectors, the testing phase can be somewhat slow. On the other hand, for low dimension problems, one could work in the embedding space and compute $\bar{w}$ once, via Eq. (4a), with the support vectors also transformed to
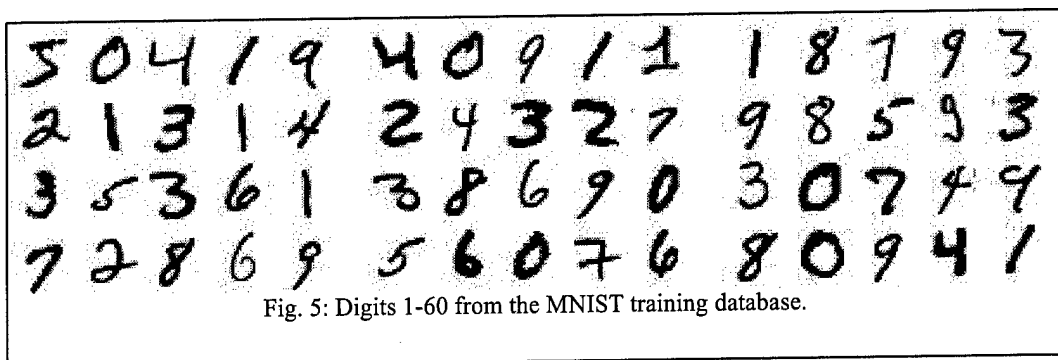
Fig. 5: Digits 1-60 from the MNIST training database.

the embedding space, as in Eq. (8). Then one can simply transform the test vector to the embedding space and compute a single dot product to classify a feature vector. The problem is dimensionality. For example, with the homogenous polynomial kernel, $K(\vec{x}, \vec{y}) = (\vec{x} \cdot \vec{y})^p$, the dimension of the embedding space is,

$$\frac{(d+p-1)!}{(d-1)!\,p!}, \tag{13}$$

where d is the dimension of the feature vector. With a 10x10 image, the feature vector has 100 elements and, using a kernel with $p=2$, results in the dimension being 5,050. However, with $p=4$, the dimension becomes 4,421,275 and so computing the feature vector in the embedding space becomes problematic. The computation of the higher dimensional feature vector is proportional to d^p, whereas the computation of the kernel is proportional to $N_s d$, where N_s is the number of support vectors. So N_s would need to be larger than d^{p-1}, in order for the kernel approach to be more computationally intensive and this would normally only occur for $p \le 2$. The boundary in Fig. 2 was found with a non-homogeneous quadratic kernel.

A potential problem can occur when the data is not separable using a given kernel. An example of this is shown in Figs. 3 and 4, where the data cannot be separated with a linear kernel, due to an outlier. Then the assumptions leading to Eq. (1) no longer hold. To overcome this, one can introduce positive slack variables δ, which measure how far the points, which are on the wrong side of the boundary, are from the optimal separating hyperplanes. The constraint equation (2) then becomes,

$$y_i(w \cdot x_i + b) - 1 + \delta_i \ge 0 \tag{14}$$

Since δ_i measures how far the corresponding point is on the wrong side of the boundary, one wants to minimize the total amount of this discrepancy, by adding it to the objective function. A convenient way to do this is to add a penalty term to the objective function. Choosing this penalty term to be the sum of the deviations, results in the Lagrangian (5) becoming,

$$\tag{15}$$

where C is a Lagrange multiplier, chosen constant C, corresponds to a higher penalty for points on the wrong side of the boundary. Setting the derivatives of Eq. (15), with respect to w and b to zero, results in the same Eqs. (4a) and (4b). Setting the derivatives to zero, results in $C = \dots$ which ... in Eqs. (4a) and (4b), and inserting into the dual Lagrangian to be the same as Eq. (5). The addition also forces to be less than C. The additional penalty term has the form given, the optimization is independent of the slack variables, so the associated Lagrange multipliers. The only effect of the additional term is to restrict the original Lagrange multipliers to, $0 \le \delta_i \le C$, instead of being simply non-negative.

Fig. 3: Linearly non-separable data with $C=\infty$. Fig. 4: data only separable data with $C=\infty$ with an

Figures 3 and 4 illustrate the non-separable case, where the data only are separable data with $C=\infty$ with an outlier added. Figure 3 shows the results of using the standard form for computing the separating hyperplane ($C=\infty$),

with a linear kernel. Notice the effect that the outlier had on the computed boundary and that nearly all the data points are support vectors. If we relax the error and choose $C=10$, then Fig. 4 results, whose separating hyperplane is closer to that of Fig. 1. In this case, the effect of the outlier has been minimized, and there are fewer support vectors required to define the boundary.

Since we had limited time and computer resources for this problem, we were not able to train the system on the entire data set. The training speed of the SVM is proportional to the number of training samples rather than the length of the feature vectors. We trained with 800 samples for each digit and even here, we used an iterative approach. First we trained on 100 sample segments and then took the support vectors from each of these and combined two at a time to train again. Using three levels of this binary tree procedure, we arrived at our final training feature vectors. The purpose of this filtering or chunking procedure was to find those feature vectors that had the best chance to be support vectors, since those vectors which are not support vectors are superfluous to the training.

Digit	0	1	2	3	4	5	6	7	8	9
0	99.0	0.0	0.2	0.5	2.7	0.6	0.4	6.2		
1	0.1	96.2	1.7	0.5	0.1	0.6	0.4			
2	0.1	0.4	91.1	1.2	0.6	0.4	0.1	0.3	0.0	1.0
3	0.1	0.2	0.6	93.5	0.0	2.9	0.0	0.2	3.5	4.6
4	0.4	0.1	0.8	0.1	94.5	0.0	1.0	3.6	1.5	3.8
5	0.2	0.1	0.3		0.1	90.2	1.1	0.8		
6	0.8	0.3	1.5	0.1	0.9		94.3	0.0	0.4	0.1
7	0.0	0.1	1.6		0.2		0.1	91.3		0.6
8	0.8	2.2	1.1	0.4	1.8	0.8	0.0		91.0	0.9
9	0.7	0.0	0.3	0.7	3.0	1.0	0.0	3.1	1.1	92.1

Table 1: Classification table for MNIST problem.

Results

In the past, we have used a variety of means to extract information from images, including statistical measures from multiresolution levels, with only limited success. We had considered using the entire image as a feature vector, instead of taking bits and pieces, but the dimensionality problem was an obstacle. The feature vector for a 32x32 image would be 1,024 elements long and would require a massive amount of training data to train a neural network, for example. However, the Support Vector Machine (SVM) has many nice properties that minimize the 'curse' of dimensionality. After extensively modifying an SVM toolbox[13], developed in MATLAB, we tested our algorithms on two data sets.

The first example was taken from the standard MNIST database[7] of handwritten digits, 0-9, which consists of a 60,000 image training set and a 10,000 image testing set. The database mixes two separate databases from NIST, one using Census Bureau employees and the other using high school students. There are approximately 250 different writers in the training set, who are different from the writers in the testing set. Samples of the images are shown in Fig. 5. As stated previously, we simply input the entire image into SVM as a feature vector. Because SVM is only a binary classifier, it is necessary to train ten separate classifiers for each digit versus all the remaining digits. To classify an image, one runs the sample through each classifier and chooses the one with the highest score. There are other ways to determine the classification from the output of each classifier[6], but we chose this 'winner take all' method for simplicity.

vectors are superfluous to the training. Training with this reduced set, gave us the parameters for the separating hyperplanes for each digit. We then used the entire 10,000 sample testing set to evaluate the classification properties of the SVM. The results of this ten class problem are shown in Table 1, where the correct values for the digits, 0-9, are in the first row and the SVM predictions are in the first column. The overall correct classification rate was over 93% on the testing set. This is quite good considering that the feature vector had 784 elements and we only used 800 training samples. In addition, note that the writing subjects in the testing set are different than in the training set. Other implementations of SVM obtain close to 1% error rates[7], when training with the full 60,000 sample training set.

Emboldened by our success with the digit classification, we turned to vehicle classification. We obtained (512x640) RGB digital images of five different vehicles (1 HMMWV and 4 trucks), taken from different positions about the front of the vehicles. To facilitate classification, we converted the images to grayscale and reduced the resolution to (16x20). Examples of the imagery, before and after, are shown in Fig. 6 and have been resized for display purposes. Since we had a limited number of images for each vehicle, we resorted to a jackknife approach for training, where we randomly chose 30 out of 50 images to train with and then tested with the remainder. We ran through 50 iterations of this and averaged the results, which are shown in Table 2. Again, the columns label the correct vehicle and the rows label the predicted vehicle. The overall classification rate was 96%.

Summary

In summary, we have outlined a relatively new method for classification problems, the Support Vector Machine (SVM). The advantages of the SVM approach are that it is a wide margin classifier which gives good results even on sparse data sets. It is outlier resistant and the training speed is independent of the vector length. The disadvantages are that the training speed increases rapidly with the number of training vectors and that the testing speed increases with the number of support vectors. These disadvantages are being addressed by the SVM community. We have shown classification results on one set of handwritten digits and the other of military vehicles. Future work consists of improving the testing speed and investigating the usefulness of preprocessing the data.

References

1) R.E. Karlsen et. al., 'Comparative study of wavelet methods for ground vehicle signature', in *Wavelet Applications*, ed. H.H. Szu, SPIE Proc. 2762, (1996).

2) R.E. Karlsen, D. Grant, R.E. Gerhart and ..... wavelet based ground vehicle acoustic recognition system', *Proc. ... Ground Target Modeling and Validation ..... Houghton, MI, 249 (.....)

3) D.J. Gorsich, R.E. Karlsen and G.R. Gerhart, 'The arrival of support vector machine and their impact on the signature community', *Fig. 6: Samples of Vehicle Imagery, original and reduced, ... Houghton, MI*, to be published (1998).

4) V. Vapnik, *The Nature of Statistical Learning*, Springer Verlag (1995).

5) C.J.C. Burges, 'A tutorial on support vector machines for pattern recognition', *Data Mining and Knowledge Discovery* 2, 1 (1998).

6) B. Schölkopf, C.J.C. Burges, and A.J. Smola, eds., *Advances in Kernel Methods, Support Vector Learning*, MIT Press (1999).

7) Y. Lecun et al., 'Comparison of learning algorithms for handwritten digit recognition', *Proc. Int. Conf. Artificial Neural Networks* II, 53 (1995).

8) D.G. Luenberger, *Linear and Nonlinear Programming*, Addison-Wesley (1984).

9) R. Fletcher, *Practical Methods of Optimization*, John Wiley and Sons (1987).

10) D.P. Bertsekas, *Nonlinear Programming*, Athena Scientific (1995).

11) W. Karush, 'Minima of functions of several variable with inequalities as side constraints', Master's Thesis, Dept. of Mathematics, Univ. of Chicago (1939).

12) H.W. Kuhn and A.W. Tucker, 'Nonlinear programming', *Proc. 2nd Berkeley Symp. On Mathematical Statistics and Probabalistics*, 481 (1951).

13) S. Gunn, 'Support vector machines for classification and regression', Technical Report, Image Speech and Intelligent Systems Group, Univ. of Southampton (1998).